

University of Kentucky

UKnowledge

---

Theses and Dissertations--Toxicology and  
Cancer Biology

Toxicology and Cancer Biology

---

2024

## THERAPEUTIC APPROACHES AND NOVEL MECHANISMS IN CANCER PROGRESSION

Kendall Simpson

*University of Kentucky*, keco244@uky.edu

Author ORCID Identifier:

<https://orcid.org/0009-0000-3531-2897>

Digital Object Identifier: <https://doi.org/10.13023/etd.2024.259>

[Right click to open a feedback form in a new tab to let us know how this document benefits you.](#)

### Recommended Citation

Simpson, Kendall, "THERAPEUTIC APPROACHES AND NOVEL MECHANISMS IN CANCER PROGRESSION" (2024). *Theses and Dissertations--Toxicology and Cancer Biology*. 57.

[https://uknowledge.uky.edu/toxicology\\_etds/57](https://uknowledge.uky.edu/toxicology_etds/57)

This Doctoral Dissertation is brought to you for free and open access by the Toxicology and Cancer Biology at UKnowledge. It has been accepted for inclusion in Theses and Dissertations--Toxicology and Cancer Biology by an authorized administrator of UKnowledge. For more information, please contact [UKnowledge@lsv.uky.edu](mailto:UKnowledge@lsv.uky.edu), [rs\\_kbnotifs-acl@uky.edu](mailto:rs_kbnotifs-acl@uky.edu).

## **STUDENT AGREEMENT:**

I represent that my thesis or dissertation and abstract are my original work. Proper attribution has been given to all outside sources. I understand that I am solely responsible for obtaining any needed copyright permissions. I have obtained needed written permission statement(s) from the owner(s) of each third-party copyrighted matter to be included in my work, allowing electronic distribution (if such use is not permitted by the fair use doctrine) which will be submitted to UKnowledge as Additional File.

I hereby grant to The University of Kentucky and its agents the irrevocable, non-exclusive, and royalty-free license to archive and make accessible my work in whole or in part in all forms of media, now or hereafter known. I agree that the document mentioned above may be made available immediately for worldwide access unless an embargo applies.

I retain all other ownership rights to the copyright of my work. I also retain the right to use in future works (such as articles or books) all or part of my work. I understand that I am free to register the copyright to my work.

## **REVIEW, APPROVAL AND ACCEPTANCE**

The document mentioned above has been reviewed and accepted by the student's advisor, on behalf of the advisory committee, and by the Director of Graduate Studies (DGS), on behalf of the program; we verify that this is the final, approved version of the student's thesis including all changes required by the advisory committee. The undersigned agree to abide by the statements above.

Kendall Simpson, Student

Dr. Xiaoqi Liu, Major Professor

Dr. Isabel Mellon, Director of Graduate Studies

THERAPEUTIC APPROACHES AND NOVEL MECHANISMS IN CANCER  
PROGRESSION

---

DISSERTATION

---

A dissertation submitted in partial fulfillment of the  
requirements for the degree of Doctor of Philosophy in the  
College of Medicine  
at the University of Kentucky

By  
Kendall Elizabeth Simpson  
Lexington, Kentucky  
Director: Dr. Xiaoqi Liu, Professor of Toxicology and Cancer Biology  
Lexington, Kentucky  
2024

Copyright © Kendall Elizabeth Simpson 2024  
<https://orcid.org/0009-0000-3531-2897>

## ABSTRACT OF DISSERTATION

### THERAPEUTIC APPROACHES AND NOVEL MECHANISMS IN CANCER PROGRESSION

Prostate cancer (PCa) remains the most diagnosed cancer among men in the United States. There are various therapeutic routes that are explored to combat this fatal disease, and our work aims to increase the options made available to PCa patients. A combination treatment of Enzalutamide (Enz), an FDA approved drug for castration-resistant PCa patients, and Metformin, an FDA approved drug for type 2 diabetes, was utilized to enhance the efficacy of Enz in Enz-resistant PCa, both *in vitro* and *in vivo*.

Thymic Lymphoma is one of the most common malignancies that can occur in various tissues and organs. Genomic stability remains a crucial cellular characteristic that prevents carcinogenesis. Within the DDR for double strand breaks (DSB), the Mre11a protein is crucial for signaling activation of ataxia-telangiectasia mutated (ATM) and performing DNA end resection during homologous recombination (HR). Our lab has demonstrated that polo-like kinase 1 (PLK1), together with casein kinase 2 (CK2), phosphorylates Mre11a during G2 DNA damage checkpoint, to prematurely terminate the DDR signaling pathway, inhibiting DNA repair during irradiation (IR) associated carcinogenesis. In this study, we aim to determine if PLK1 phosphorylation of Mre11aSSDD can prevent radiation-induced carcinogenesis *in vitro* and *in vivo*.

KEYWORDS: Prostate cancer, drug-resistance, oxidative phosphorylation, Mre11a, ionizing radiation, PLK1

---

Kendall Elizabeth Simpson

---

07/15/2024

Date

THERAPEUTIC APPROACHES AND NOVEL MECHANISMS IN CANCER  
PROGRESSION

By  
Kendall Elizabeth Simpson

Dr. Xiaoqi Liu  
\_\_\_\_\_  
Director of Dissertation

Dr. Isabel Mellon  
\_\_\_\_\_  
Director of Graduate Studies

07/15/2024  
\_\_\_\_\_  
Date

To my younger self who chose to open this difficult chapter of life and who grew into a resilient person by the end of it.

## ACKNOWLEDGMENTS

First and foremost, I would like to thank my mentor, Dr. Xiaoqi Liu, for allowing me to complete my Ph.D. in his lab, his continued support in advancing my career, and for his mentorship. Similarly, I would like to thank my committee members, Dr. Chunming Liu, Dr. David Orren, and Dr. Yakaterina Zaytseva for their continued advice, education, time, and knowledge as their criticism was crucial for the completion of this dissertation. I would like to thank my outside examiner and previous committee member, Dr. Brett Spear, for the countless hours he spent listening to seminar practices, reading documents, comprehending my projects, and continued positive attitude. Along with Dr. Spear, Dr. Brittany Rice poured into me so much of her personal time and mental space as a friend and as a peer mentor. Her reminders that completing a Ph.D. in academia is a beast by itself without the added stress of life were helpful in normalizing my experiences. Not only do I want to thank Dr. Liu's lab, as a whole, for their mentorship and comradery, but particularly, I would like to thank Dr. Yanquan Zhang, Dr. Zhiguo Li (before and after he was promoted to PI), Dr. ZhuangZhuang Zhang, Xinyi Wang, Tempany Arbogast, Mohammad Esfini Farahani, and Amos Olalekan Akinyemi. These individuals mentored, gave advice, and demonstrated a tremendous amount of kindness when times got tough. I would also like to thank Dr. Katelyn Jones, who quickly became a close friend and was with me every step of the way as we finished this academic journey. Her friendship is a gift and was a necessity while finishing this degree and for that, I couldn't thank her more for her time and kindness

Next, I would like to thank my family for their unwavering support and love during this chapter in my life. Two of my younger sisters, Kayla and Katie, both had beautiful sons and a daughter while I completed my education. Getting the opportunity to watch them become mothers and be a part of my niece and nephews' lives has been such a rewarding experience and I can't wait to spend more time with them in the future. I want to thank my youngest sister, Kelsey, for her quality time and choice words, always counting on her for the quick-witted joke to pick me up. I want to thank my stepfather, Ricky D, who never missed a chance to tell me how proud he is of me. Even when I couldn't see my accomplishments for what they were, he always reminded me of how much I have done and how far I have come. I want to thank my mama, not only for answering my countless phone calls and listening to my many tears along the way, but also for having confidence in me and in my resilience to finish the task I had set my mind to. I'm so glad she walked over to the McNair Scholars table at the ECU open house, putting the idea of getting a Ph.D. on the table for me in the first place.

Finally, and most importantly, I would like to thank my husband, Justin. Not only have we both grown as people astronomically during this portion of my education, but he has never stopped trying to be my rock, my support, my person. I can't imagine what this would have been like without his constant words of encouragement and the partnership we have built together. I can't wait to continue to spend the rest of my life with him.

## TABLE OF CONTENTS

ACKNOWLEDGMENTS .....	iii
LIST OF FIGURES .....	viii
CHAPTER 1. Introduction .....	1
1.1 <i>Review of Prostate Cancer</i> .....	1
1.1.1 Introduction.....	1
1.1.2 Disease etiology .....	2
1.2.3 PCa treatment and castration-resistant prostate cancer.....	3
1.2.4 AR Signaling in PCa .....	4
1.2.5 PCa glucose metabolism and treatment vulnerability .....	6
1.2.6 Metformin .....	7
1.1.6 Conclusion of using combination therapies in PCa .....	8
1.2 <i>Mre11a</i> .....	9
1.2.1 Genomic instability in cancer.....	9
1.2.2 DNA repair subtypes .....	10
1.2.3 Mre11a in DSB repair .....	11
1.2.4 Cellular function and regulation of PLK1 .....	12
1.2.5 Regulation of Mre11a via phosphorylation by PLK1 .....	13
1.2.6 Thymic lymphoma as a model to observe changes in DDR .....	13
CHAPTER 2. Overcoming therapy resistance of CRPC <i>in vitro</i> via metformin combination treatment with enzalutamide .....	15
2.1 <i>Overview</i> .....	15
2.2 <i>Introduction</i> .....	16
2.3 <i>Materials and Methods</i> .....	18
2.3.1 Cell Culture, Chemicals, and Reagents.....	18
2.3.2 Clonogenic Assay.....	19
2.3.3 Cell Viability and Synergy.....	19
2.3.4 Protein Immunoblotting.....	19
2.3.5 Seahorse Analysis.....	20
2.3.6 Flow Cytometric Analysis .....	21
2.3.7 RNA Sequencing Analysis.....	21
2.3.8 22Rv1-derived Xenograft Mouse Model .....	22
2.3.9 LuCaP35CR Xenograft Mouse Model .....	22
2.3.10 Histology and Immunohistochemistry .....	23
2.3.11 Statistical Analysis.....	23

2.4 Results.....	23
2.4.1 Metformin treatment exhibits a synergistic effect with enzalutamide in ENZ-r CRPC lines. ....	23
2.4.2 Combination treatment results in metabolic reprogramming .....	24
2.4.3 Combination treatment effect on 22Rv1-derived xenograft tumors ....	27
2.4.4 Combination treatment effect on LuCaP35CR xenograft tumors.....	28
2.4.5 RNA Sequencing analysis of isogenic ENZ-r CRPC lines. ....	28
2.5 Discussion.....	29
CHAPTER 3. The regulation of Mre11a via Plk1 phosphorylation in thymic lymphoma .....	41
3.1 Overview.....	41
3.2 Introduction .....	42
3.3 Materials and Methods.....	44
3.3.1 Mouse Lines and Genotyping.....	44
3.3.2 Tamoxifen Treatment and Total Body Irradiation (TBI).....	46
3.3.3 Flow Cytometric Analysis .....	46
3.3.4 Complete Blood Count .....	47
3.3.5 Histological and Immunohistochemical (IHC) Analysis.....	47
3.3.6 Establishment of Mouse Embryonic Fibroblasts (MEFs) .....	47
3.3.7 Immunoblotting.....	48
3.3.8 Immunofluorescence .....	48
3.4 Results.....	49
3.4.1 Split low dose radiation-induced carcinogenesis model. ....	49
3.4.2 Carcinogenesis was not different between WT and Mre11a <sup>SSDD</sup> mice following split low dose radiation. ....	50
3.4.3 scRNA sequencing preliminary analysis suggests a possible difference between Mre11a <sup>SSDD</sup> mice and WT after split low dose radiation.....	53
3.4.4 Medium-high single dose treatment has no effect on the development of carcinogenesis in either Mre11a <sup>SSDD</sup> or WT mice.....	53
3.4.5 Mre11a <sup>SSDD</sup> MEFs promote extension of $\gamma$ H <sub>2</sub> AX induction immediately following IR.....	54
3.4.6 Lethal dose of IR induced survival does not differ between WT and Mre11a <sup>SSDD</sup> mice.....	55
3.5 Discussion.....	56
CHAPTER 4. Conclusion and future directions .....	69
4.1 Conclusion .....	69
4.2 Future Directions.....	75

APPENDIX .....	78
REFERENCES .....	80
VITA .....	99

## LIST OF FIGURES

Figure 2.1 Enzalutamide and Metformin in combination synergistically inhibit growth of enzalutamide resistant CRPC <i>in vitro</i> .....	33
Figure 2.2 Combination treatment results in metabolic reprogramming.....	35
Figure 2.3 Combination treatment of enzalutamide and metformin did not attenuate 22Rv1 Xenograft tumor growth <i>in vivo</i> .....	37
Figure 2.4 Combination treatment of enzalutamide and metformin did not attenuate LuCaP35CR tumor growth <i>in vivo</i> .....	39
Figure 2.5 RNA sequencing analysis of isogenic CRPC lines.....	40
Figure 3.1 Experimental design and thymic lymphoma monitoring of split low dose irradiation mice following treatment.....	59
Figure 3.2 IHC images and flow cytometric analysis of split low dose irradiation mice at harvest.....	62
Figure 3.3 scRNA-seq analysis suggests a possible RNA expression difference between both IR treated experimental groups.....	64
Figure 3.4 Single dose radiation at 5Gy does not exhibit a radiation-induced carcinogenesis phenotype.....	65
Figure 3.5 Mre11a <sup>SSDD</sup> MEF DDR response to double strand break damage.....	66
Figure 3.6 Survival curve analysis of Mre11a <sup>SSDD</sup> mice.....	68

## CHAPTER 1. Introduction

### 1.1 Review of Prostate Cancer

#### 1.1.1 Introduction

PCa remains to be the most commonly diagnosed cancer among men in the United States (US) [1]. Diagnoses of PCa are predicted to escalate, illustrating the necessity for the novel development of therapeutic strategies [2]. After surgical and radiation intervention, androgen deprivation therapy (ADT) is the next line of treatment for PCa patients, unfortunately reoccurrence, often with metastatic properties, remains an issue [3]. This led to the development of Enzalutamide, a clinically used second generation AR inhibitor, that directly binds to AR and prevents cell proliferation [4]. Even with advanced strategies to combat this disease, patients gain resistance to this line of treatment and are left with minimal therapeutic options. This has led researchers to exploring and repurposing various FDA-approved medications in hopes that discovery a viable therapeutic outcome for Enz-resistant CRPC.

In recent studies, it has been seen that there is a metabolic switch in drug resistant PCa, indicating a shift from reliance on aerobic respiration to aerobic respiration [5]. To capitalize on this vulnerability, utilization of therapeutics that inhibit oxidative phosphorylation may be a novel avenue in treatment strategies [6]. Metformin, a commonly used FDA approved therapy for the treatment of type 2 diabetes and will be discussed later in detail, has recently come to light as a possible treatment strategy for many types cancers, in particular, PCa [7].

### **1.1.2 Disease etiology**

As recent reports indicate, PCa leads as the highest estimated new cancer cases in men in the United States and the second leading cause of cancer deaths [1]. Prostate cancer is typically characterized by late age diagnosis and slow disease progression [8]. Age is the number one risk factor in the development of prostate cancer, while race and a genetic predisposition also plays a large role in disease incidence [9]. AR signaling pathway plays a critical role in PCa disease initiation and progression, and is considered the main driver of PCa, however, there are various other mechanisms in which PCa progresses. Germline mutations in critical genes such as *ATM*, *BRCA2*, and *HOXB13* leave patients with a higher predisposition for the development of advanced prostate cancer, in particular, metastatic PCa [10]. In addition, patients with single nucleotide polymorphisms (SNPs) variants in cancer-related pathways also play a role in the initiation of this disease [11]. Following these genetic mutations and variations, the progression of PCa typically goes unnoticed for some time, as men with early stages of PCa are asymptomatic and are often overlooked [12]. Symptoms related to the urinary tract can often be easily dismissed or in some cases, not related to a malignancy in the prostate and rather a benign hyperplasia (BPH), which causing trouble urinating and general discomfort [13]. As PCa continues to progress, men in later stages of this disease may experience symptoms including bone pain in the hips, back, and pelvis as well as varying degrees of incontinence which can lead to even further disease complications [12]. One of the critical tests for the initial diagnosis of PCa is a blood serum test for the detection of prostate specific antigen (PSA) levels in

blood circulation [14]. PSA, typically only observed in the prostate gland, can enter circulation following the breakdown of the basal membrane of the prostate gland during disease progression [15]. In general, biomarkers for cancer subtypes are rare and sometimes unreliable, however, this PSA biomarker is critical for determining disease progression. Following initial treatments for PCa, a second rise in serum PSA is a critical observation for determining cancer recurrence and a need for changing therapeutic strategies [16].

### ***1.2.3 PCa treatment and castration-resistant prostate cancer***

Depending on cancer stage, genetic factors, and recurrence, PCa treatments will vary vastly between patients or progression [17]. In the case of localized PCa, radical prostatectomy, or surgical removal of the prostate gland, coupled with radiation therapy, is standard of care [18]. This treatment will typically decrease serum PSA and temporarily halt disease progression. Despite these treatments, a rise in serum PSA can indicate disease progression. Unfortunately, this leads clinicians to modify their treatment plans. Since AR activation is a prominent event in the initiation and activation of PCa, prevention of this signaling is imperative. This leads clinicians to recommend chemical or surgically castration, in order to deplete the patient's body of androgen and decrease AR activation. Though this approach works for a time being, AR contains the ability to switch on through various signaling pathways. This leads the disease into a category labeled CRPC [19]. CRPC patients are typically treated with ADT to either inhibit AR signaling directly or to prevent androgen synthesis, resulting in a prevention of disease progression [20]. Despite the initial success of ADT, PCa has the capability to

develop alternative mechanisms of tumorigenesis independent of AR signaling, categorizing it as mCRPC [21]. Within mCRPC, a recent report has categorized 4 different types of CRPC; AR-dependent, neuroendocrine (NE), Wnt-dependent, and stem cell-like CRPC [22]. Based on the results from this study, AR-dependent CRPC is characterized with high expression of AR and chromatin accessibility of AR-target genes such as *KLK2* [23]. NE CRPC samples have a high expression of the *SYP* gene which codes for proteins critical in adrenal function, as well as a phenotype similar to small-cell carcinoma [24]. Both Wnt-dependent and stem cell-like CRPC have low expression of AR and NE genes and are harder to treat despite recent understanding [25-27]. Regardless of subtype of CRPC, these genetic phenotypes of disease aid clinicians in the continued treatment of PCa. As the disease becomes more severe, treatment options become more limited and often, patients with CRPC are treated with second-generation AR inhibitors (sgARi) such as apalutamide, darolutamide, and enzalutamide [28]. Of these, enzalutamide is currently the only therapy approved for metastatic CRPC, however, these therapies only extend patient survival, and drug-resistance still occurs [29]. It is critical to determine novel treatment strategies for this niche of advanced drug-resistant mCRPC in order to increase overall patient survival and quality of life.

#### ***1.2.4 AR Signaling in PCa***

Although there are numerous mechanisms in which cancer can be initiated such as carcinogen exposure, mutation accumulation, and other factors; PCa initiation is typically characterized by gene alterations within the AR signaling axis

[30]. Alterations in AR signaling plays a pivotal role in the development and progression of PCa; however, AR signaling in homeostasis is critical for the development and maintenance of the prostate gland [31]. Canonically, testosterone and dihydrotestosterone (DHT) are the most predominant androgens in the development and maintenance of reproductive tissues [32]. Coincidentally, both testosterone and DHT can bind to AR in the cytoplasm as ligands activating AR signaling [31]. In the absence of AR ligand, AR is bound to chaperone heat shock proteins (HSP) -90, -70, -56 and other chaperone proteins modulating the transcriptional activity of AR [33]. Following ligand binding, AR will undergo a conformational change initiating AR homodimerization and ultimately, AR nuclear translocation [34]. AR, upon entering the nucleus, will recognize specific androgen response elements (ARE) in the promoter/enhancer regions of targeted genes. AR in this context functions as a transcription factor for genes such as PSA or probasin, a prostate-specific gene that acts as a marker for prostate differentiation and elucidates androgen action [35]. In the case of PCa, the transcriptional activity of AR on AREs can also initiate the transcription of other cancer-related genes contributing to disease progression [36].

There are several mechanisms by which aberrant AR signaling can induce PCa initiation and progression, the most common being splice variants of AR [37]. It has been reported that during the maturation of mRNA, splice variants of AR lacking a ligand binding domain (LBD) occur often rendering the variant constitutively active leading to poor survival rates [38]. AR-V7, one of the most abundant variants of AR, is truncated at the end of exon 3 and lacks the LBD and

therefore can remain active in a ligand-independent manner [39]. AR-V7 still possesses the DNA-binding domain and nuclear localization signal of AR thereby retaining the transcriptional factor functions of AR and produces difficulties in treatment. PCa that possess these splice variants are intrinsically resistant to direct AR inhibitors such as enzalutamide [40]. In addition, the inordinate expression of AR can also be attributed to the biosynthesis of androgens, of which treatments such as abiraterone aim to inhibit. Despite various treatment options and strategies, PCa can develop methods in which to overcome these challenges and drug-resistance remains an issue of concern.

#### ***1.2.5 PCa glucose metabolism and treatment vulnerability***

It is well known that many cancers exhibit what is considered the “Warburg Effect” which describes the altered means in which cancer cells undergo glucose metabolism [41]. Cancer cells tend to rely on aerobic glycolysis and therefore lactate production as the main method in utilizing glucose. Lactate fermentation is a less efficient method in which adenosine 5'-triphosphate (ATP) can be produced from a single molecule of glucose and bypasses the need for the mitochondrial production of ATP [42]. This is the opposite method in which normal cells utilize glucose where aerobic respiration occurs and the cells rely on oxidative phosphorylation (OX PHOS) to produce the majority of the cell's energy needs [5]. The utilization of glycolysis, pyruvate oxidation, the Krebs cycle, and OX PHOS to produce the ATP needed to maintain cellular function is different in cancer cells and the reasoning is still unknown [43]. In the case of advanced PCa, it has been recently documented that these cancer cells rely on OX PHOS rather than lactate

production [5]. PCa cells utilize a proton gradient in the inner mitochondrial membrane to drive chemiosmosis and thereby ATP production, therefore many complex proteins in the electron transport chain are critical for this process [44]. These differences in glucose metabolism introduce a possible vulnerability in the cancer cells that may be exploited in novel treatment strategies.

### **1.2.6 Metformin**

One possible mechanism in which we can inhibit OX PHOS is the administration of metformin. Metformin is a biguanide which was originally approved for the treatment of non-insulin dependent diabetes mellitus, or type 2 diabetes, in 1994 [45]. For patients with type 2 diabetes, metformin is utilized to control glycemia by lowering blood glucose levels in the presence of insulin resistance [46]. Metformin's primary mechanism of lowering blood glucose levels comes from decreasing hepatic glucose output and thereby reducing gluconeogenesis [45]. Specifically, metformin activates the AMP-activated protein kinase (AMPK) which plays a critical role in maintaining energy homeostasis in the cell [47]. Ultimately, following activation of AMPK, the cell will switch from an anabolic state to a catabolic state shutting down energy synthesis pathways and restoring energy balance [47]. In addition to metformin's effect on AMPK, metformin has been observed to also inhibit complex I in the electron transport chain of OX PHOS preventing ATP production via chemiosmosis effectively impacting aerobic respiration [48].

The concept of utilizing metformin as a cancer treatment gained traction after the observation that diabetic patients taking metformin had a decreased cancer

incidence and cancer-related mortality [49]. In addition, as the most commonly prescribed therapy for type II diabetes patients, metformin has an excellent safety profile with limited side effects [50]. In recent years, investigation of metformin treatment, particularly in PCa, has been explored as a possible treatment option for advanced CRPC [51]. As an inhibitor of OX PHOS, metformin may be useful in treating advanced CRPC as a method for exploiting the abnormal mechanism of glucose metabolism for cancers. In addition, the metformin-mediated activation of the AMPK pathway has been shown to inhibit the activation of the mammalian target of rapamycin (mTOR) and protein synthesis pathways [52]. Considering the effect of metformin on glycemic control, how is it that we can speculate the use of metformin as a cancer treatment despite the absence of non-insulin dependent diabetes mellitus? Recent reports indicate that metformin's anti-tumorigenic effects are independent of its effects in glycemic control, however, metformin is considered safe for use in the literature despite hypoglycemic events that can occur from taking this drug [53].

#### ***1.1.6 Conclusion of using combination therapies in PCa***

The logistics in the development of novel therapeutic drugs comes with a monumental financial cost and investment of time, therefore, developing treatment strategies that utilize FDA-approved drugs with promising safety profiles are an attractive target for cancer therapeutics [54]. Utilization of FDA-approved therapies continues to be a topic of interest in the development of novel treatment strategies as these drugs have already been approved and tested for safety and toxicity in humans [55]. In the case of PCa, enzalutamide exhibited high efficacy both in

clinical trial and in practice, despite the observation of resistance in advanced CRPC. Historically, combination treatment approaches have assisted in overcoming certain resistant obstacles and provided late-stage patients with additional options. Ideally, combination treatments possess the ability to attack various targets in order to control or slow the growth of the malignancy [56]. In this study, we aimed to combine metformin with enzalutamide treatment as a means of increasing the efficacy of enzalutamide as well as repurposing an FDA-approved to halt the energy production to the cancer cell.

## **1.2 Mre11a**

### ***1.2.1 Genomic instability in cancer***

Historically, the importance of maintaining genomic stability has been investigated for decades and is a foundational concept in the maintenance of homeostasis. Evolutionarily, proteins critical for DNA repair and maintenance are largely conserved across species from yeast to humans which highlights the importance of regulation of this intricate cellular process [57]. As a hallmark of cancer, genomic instability can occur in different mechanisms such as TP53 inactivation pathways and mutations in caretaker genes such as tumor suppressors and oncogenes [58]. The critical role of the DDR is to prevent mutations by repairing damaged DNA, however, some mutations are hereditary. Certain germline mutations, such as BRCA mutations in breast cancer, are passed from parental genetics and therefore, the breast cells of these patients are more vulnerable to developing cancer [59]. In this example, BRCA genes are tumor suppressors, so when mutated, DNA repair is inhibited and irregularities occur in

DNA synthesis [60]. Similarly, many other cancers depend on the alteration of the DNA damage response to induce a cancerous phenotype [61].

In contrast, many therapeutics on the market aim to induce DNA damage in the cancer to induce apoptosis and cell death [62]. Cisplatin, a commonly used platinum drug for the treatment of various cancer, is demonstrated to induce nephrotoxicity in treated cells by forming cisplatin adducts [63]. By forming interstrand crosslinks in the DNA, the treated cells either need to attempt to repair the DNA or if the damage is too great, simply progress to apoptosis [64]. By this mechanism, cisplatin affects cancer cells, however, as normal cells also have DNA, there are unwanted side effects [64]. There are many other agents that have a mechanism of action like cisplatin in that they disrupt the genomic stability and induce cell death, highlighting the importance of genome maintenance.

### ***1.2.2 DNA repair subtypes***

Historically, there are 5 main subtypes of DNA damage repair, 2 of which repair double strand breaks and the other 3 typically repair single strand breaks [65]. There are many nuances between nucleotide excision repair, base excision repair, and mismatch repair of which all of them recognize different DNA damage lesions, however, all 3 of these pathways typically repair single strand breaks [66]. Homologous recombination (HR) and non-homologous end joining (NHEJ) are the 2 primary mechanisms in which cells repair DSB damage [67]. In the case of DSB, both the parental and daughter strand of DNA are severed leaving either a clean break where homologies are close in proximity to each other or larger DSB where sections of the DNA are either missing or removed. HR relies on utilizing the

overhanging strands of both strands of DNA to identify the homologies and repairs the damage in a relatively error-free manner [68]. In the case where DNA damage is so large and homologies/sections of DNA are lost, NHEJ will simply repair the DNA by trimming and ligating the ends together, however, this will most likely result in mutations, gene loss, chromosomal rearrangements, or other genomic alterations [69].

### **1.2.3 *Mre11a* in DSB repair**

*Mre11a*, a critical protein in the MRN complex, is crucial for both HR and NHEJ pathways of DSB repair. At both stalled replication forks and sites of DSB damage, meiotic recombination 11 homolog 1 a (*Mre11a*) protein forms a complex with Rad50 and Nbs1 called the MRN complex, orchestrating some of the first responses in the DDR [70]. NBS1 is first recruited to the site of DNA damage through the interaction with cell cycle checkpoint protein Rad17 [71]. Once at the site of damage, MRN will recruit and activate ATM and ATR for further downstream DDR signaling [72]. Finally, activated ATM phosphorylates mediator of DNA damage checkpoint 1 (MDC1) protein for continued amplification of the signal and recruitment of additional MRN complexes [73]. The intricacies of NHEJ and HR repair differ in proteins involved both upstream and downstream, however, the MRN complex and signaling activation of ATM/ATR are present in both types of repair.

In NHEJ, DSBs are mended by DNA end joining with minimal processing. Within this process, Ku heterodimer, consisting of both Ku70 and Ku80 will bind at the DNA ends and recruit DNA-PKCs which are critical for phosphorylates various

proteins responsible for DNA end processing and ligation [74]. The initial DNA end resection requires both the endonuclease and exonuclease activity of the MRN complex as well as other enzymes, such as CtIP, PARP1, FEN1, and DNA ligases I and III for the completion of repair or regulation of the process via WRN or BLM helicase [75-77].

In HR, DSBs are extensively resected, specifically creating 3' ssDNA overhangs which in turn prevents NHEJ [78]. Mre11a, within the MRN complex, will initiate and license DNA resection through endonuclease activity by creating a nick for the exonuclease activity to resect the DNA in a 3' to 5' direction [79]. At the nick, 5' to 3' nucleases such as EXO1 and helicases such as BLM or WRN will promote extended resection away from the nick and create a 3' overhang of DNA [80]. This process creates the homologies needed for homologous recombination and ultimate DNA repair [77].

#### ***1.2.4 Cellular function and regulation of PLK1***

Polo-like kinase 1 (PLK1), an essential protein in the regulation of cell cycle, has been demonstrated as highly upregulated in cancers [81-83]. Canonically, PLK1 is a key mitotic regulator where it functions in regulating mitotic entry, centrosome maturation, spindle assembly, APC/C regulation and Cytokinesis [84]. Typically, transcriptional levels of PLK1 are tightly regulated in G1 phase by tumor protein P53, cyclin-dependent kinase inhibitor 1, and retinoblastoma protein [85]. It has been reported that p53 and p21 regulate the expression of PLK1 via direct binding with PLK1 preventing its transcription [86]. As evidence has grown

demonstrating that PLK1 may play a role in various cancer progression and initiation, non-canonical functions of PLK1 have been explored.

### **1.2.5 Regulation of Mre11a via phosphorylation by PLK1**

Generally, the phosphorylation of Mre11a is essential for progressing many critical functions of DSB repair as well as affecting cell cycle and chromosomal rearrangement [87]. Mre11a can be phosphorylated by Cdk1 during mitosis suggesting the necessity of Mre11a activation during cell cycle [88]. Following these implications, our lab sought to understand if PLK1 also played a role in the regulation of Mre11a. Through *in vitro* kinase assays, our lab was able to demonstrate that PLK1 phosphorylates Mre11a at S649 during G2 phase DNA damage recovery [89]. In addition, PLK1-mediated phosphorylation enhances the subsequent phosphorylation of Mre11a at S689 by CK2 and these two phosphorylation events drive premature checkpoint termination and reduced DNA repair [89].

### **1.2.6 Thymic lymphoma as a model to observe changes in DDR**

As DNA DSB can be an effective means in which to induce mutagenesis, various DNA damage inducers are utilized in cancer therapies, particularly, ionizing radiation damage. In the treatment of carcinogenesis, scientists and clinicians have utilized ionizing radiation (IR) to induce DNA damage as a means of inducing apoptosis in cancer cells [90]. IR treatments can be an effective means in which to treat carcinogenesis, however, patients often experience severe side effects including secondary cancer formation [91]. The current gold standard model in studying the mechanisms of radiation-induced carcinogenesis, utilizing a

fractionated low dose radiation exposure treatment [92]. In addition to understanding carcinogenesis mechanisms, it is also understood that split low dose irradiation is a reliable method for the induction of thymic lymphoma [93]. One of the benefits of utilizing the split low dose irradiation model in investigating DNA repair responses to DNA damage, is the ease in which disease progression can be monitored. In thymic lymphoma, T cells developed in the thymus, are normally in an immature state expressing CD8a and CD4 simultaneously [94]. Following release from the thymus, mature T cells express either CD8a, CD4, or neither in a normal system. In the case of thymic lymphoma, immature T cells, expressing CD8a and CD4 together are found in circulation as an indicator of disease progression [95]. These T cell changes are normally in response to an accumulation of DNA damage within the hematopoietic system which is indicative of an increased mutational burden and a lack of DNA repair.

## CHAPTER 2. Overcoming therapy resistance of CRPC *in vitro* via metformin combination treatment with enzalutamide

### 2.1 Overview

Prostate cancer remains the most diagnosed cancer among men in the United States with approximately 268,500 new cases a year [1]. Following surgery/radiation, ADT is the standard treatment for castration-sensitive prostate cancer (CSPC) patients. However, recurrence and metastases after ADT remain an issue and patients are then categorized as CRPC [96]. Enzalutamide, an FDA approved drug currently prescribed to patients with CRPC, inhibits AR nuclear translocation and prevents AR transcriptional activity [28]. This therapy is a typical approach to treating CRPC and due to continuous reliance on the drug, can lead to Enzalutamide-resistance (ENZ-r) [97-99]. This highlights the necessity for developing novel therapeutic targets to combat the gain of resistance.

Metformin, a common FDA approved therapy for type 2 diabetes, has been recently investigated for its potential anti-tumorigenic effects in many cancer types [49]. In this study, we used enzalutamide and metformin in combination to explore the possible rescued efficacy of enzalutamide in the treatment of ENZ-r CRPC. We first tested the effects of this combination treatment on cell viability, drug synergy, and cell proliferation in ENZ-r CRPC cell lines. After combination treatment, we observed a decrease in cell proliferation and viability as well as a synergistic effect of both enzalutamide and metformin *in vitro*. Following these results, we sought to explore how combination treatment effected mitochondrial fitness utilizing mitochondrial stress test analysis and MMP shifts due to metformin's action in

inhibiting Complex I of oxidative phosphorylation. While deciphering the effects of combination treatment on mitochondrial function *in vitro*, we employed 2 different strategies of *in vivo* testing using 22Rv1 and LuCaP35CR xenograft models. Finally, drug-resistant CRPC lines were subjected to combination or mono treatments and subsequent RNA sequencing to determine a possible mechanism of vulnerability of the combination treated cells. RNA sequencing revealed a potential link in the downregulation of Ras/MAPK signaling following combination treatment.

## **2.2 Introduction**

Prostate cancer (PCa) has the highest number of new cases in men in the United States with approximately 288,300 new cases in 2023 and is the second leading cause of cancer related deaths with an estimated 34,700 deaths in 2023 [1]. Early stage PCa patients that undergo localized therapies, radical prostatectomy, and hormone therapies will often experience cancer regression and symptom relief [18]. Hormone therapy, commonly referred to as androgen deprivation therapy (ADT), is utilized to prevent androgen receptor (AR) signaling and therefore PCa progression, however, over time many patients will often experience recurrence and are considered to have castration-resistant prostate cancer (CRPC) [3, 19]. Upon cancer recurrence, therapeutic options become more limited, and patients will often be treated with FDA-approved AR inhibitors such as abiraterone, enzalutamide, and darolutamide. In the case with metastatic CRPC, the only FDA-approved AR inhibitor available is enzalutamide, however, most patients being treated with enzalutamide over time will experience enzalutamide

resistance [97-99]. This evidence demonstrates the critical need for the development of novel treatment strategies in advanced drug resistant CRPC.

In recent years, metformin, the most commonly prescribed oral biguanide to treat type II diabetes, has gained traction with its implications in reduced cancer risk and potential utilization as cancer treatments [100, 101]. Metformin has limited side effects and an excellent safety profile so investigation into possible drug-repurposing as a cancer therapy is an attractive option in many cancer types [54]. In addition to numerous mechanistic studies in PCa utilizing metformin as a cancer therapy [102-105], there have been multiple clinical trials in recent years exploring this mechanism of cancer treatment [106, 107]. In particular, a phase II clinical trial in Switzerland utilized combination treatment of enzalutamide and metformin in CRPC patients who have never been exposed to enzalutamide and other endocrine agents [108]. While there is validity in utilizing enzalutamide and metformin in combination for CRPC patients, there is little known about this combination treatment in drug-resistant CRPC.

In this study, we found that combination treatment of enzalutamide and metformin in established drug-resistant CRPC lines demonstrate a synergistic anti-proliferative effect *in vitro*. In addition, we investigated the effect of combination treatment on mitochondrial function utilizing a mitochondrial stress test seahorse assay and measuring the mitochondrial membrane potential (MMP), however, we did not observe any significant effects on drug-resistant CRPC lines. To validate our synergy results *in vivo*, we employed two different xenograft models to determine the effects of combination treatment on tumor growth, however, we did

not observe a difference in tumor growth between treatment groups. Finally, we treated drug-resistant CRPC lines with combination therapies for RNA sequencing to determine a mechanistic link. Together, these results highlight the importance of utilizing robust models in cancer research to test novel treatment strategies.

## **2.3 Materials and Methods**

### **2.3.1 Cell Culture, Chemicals, and Reagents**

LNCaP, MR49F, C4-2, C4-2R, and 22Rv1 cell lines were used in this study. LNCaP cells are androgen-dependent cells, however, C4-2 cells were derived from LNCaP cells and are androgen independent. In a similar fashion, MR49F cells are also derived from LNCaP cells, however, MR49F cells are enzalutamide resistant. C4-2R cells are enzalutamide resistant cells derived from C4-2 cells. C4-2 cells were obtained from the M. D. Anderson Cancer Center whereas MR49F and C4-2R cells were kindly provided by Dr. Amina Zoubeidi at the Vancouver Prostate Cancer Center and Dr. Allen Gao at University of California at Davis, respectively. LNCaP and 22Rv1 cells were purchased from ATCC. All cells were cultured in RPMI-1640 media supplemented with 10% (v/v) fetal bovine serum, 100 units/mL penicillin, and 100units/mL streptomycin incubated at 37°C and 5% CO<sub>2</sub>. MR49F and C4-2R were maintained in 10mM and 20mM enzalutamide solution, respectively to maintain resistance. Enzalutamide was purchased from MedChemExpress (HY-70002). Metformin HCl, Onvansertib [NMS-P937], and Carbonyl cyanide-4-(trifluoromethoxy) phenylhy-drazone [FCCP] were purchased from Selleckchem (S1950, S7255, S8276).

### **2.3.2 Clonogenic Assay**

MR49F, C4-2R, and 22Rv1 cells were seeded ( $3-6 \times 10^3$ /well) into 6-well plates with 3mL of RPMI-1640. The following day, cells were treated with varying drugs as indicated and incubated at 37°C. Cells were treated every other day for 10 days, then then washed with ice cold 1X PBS, fixed with ice cold methanol for 10 minutes on ice, and stained with 0.5% crystal violet staining solution. Relative well intensity was calculated using ImageJ software.

### **2.3.3 Cell Viability and Synergy**

MR49F, C4-2R, and 22Rv1 cells were seeded ( $6 \times 10^3$ /well) into 96-well plates with 100mL of RMPI-1640. 24 hours later, cells were treated with varying drugs at the indicated concentrations and allowed to incubate for 72 hours. To assess cell viability, AquaBluer solution (also known as Alamar Blue) was added to each well in a 1:100 ratio of AquaBluer solution: culture media, which monitors the reducing environment of the living cell. Cells were incubated for 4 hours at 37°C before measuring the fluorescent intensity 540ex/590em via GloMax Discover microplate reader (Promega). Cells were seeded in quadruplicate for each drug concentration and the readings were all normalized to average blank control wells without cells. The results are expressed as the percentage of viable cells with respect to the negative control (DMSO) which represents 100% viability shown above. Synergy scores were calculated using SynergyFinder.org.

### **2.3.4 Protein Immunoblotting**

Cells were previously treated with varying drug combinations for 48 hours before harvest. Cell lysis was achieved by 10% RIPA solution with protease and

phosphatase inhibitors followed by sonication. Protein concentration was measured by Pierce BCA Assay kit and equal concentrations of protein lysate from each sample were mixed with SDS loading buffer, resolved on an SDS-Page gel electrophoresis, and transferred to either Nitrocellulose or PVDF membranes followed by blocking and incubation with primary and HRP-conjugated secondary antibodies. ECL was used to induce chemiluminescence and membranes were imaged using BioRad ChemiDoc MP. BioRad ImageLab software was utilized to analyze immunoblots.

### **2.3.5 Seahorse Analysis**

MR49F, C4-2R, and 22Rv1 cells were seeded ( $2 \times 10^4$ /well) into XFe96 cell culture microplates in RPMI-1640 culture medium and incubated for 24 hours. Cells were then treated with varying drug concentrations as indicated for 24 hours prior to analysis. Both the Oxygen consumption rate (OCR) and the extracellular acidification rate (ECAR) were measured using the seahorse XFe96 analyzer from Agilent. Mitochondrial stress test was performed by first measuring the initial OCR rate for cells, followed by  $1 \mu\text{M}$  oligomycin which inhibits complex V of oxidative phosphorylation (indicative of the ATP production rate). Next,  $1-2 \mu\text{M}$  of FCCP treatment was used to uncouple the proton gradient and determine maximum respiration (FCCP titration experiment to determine optimal FCCP dose was conducted prior to analysis). Following this,  $1 \mu\text{M}$  of both rotenone and antimycin A were given, which inhibits complexes I and III, respectively.

### **2.3.6 Flow Cytometric Analysis**

For measuring mitochondrial membrane potential, cells were seeded (between  $5 \times 10^5$  and  $1 \times 10^6$ /well) into 6 well plates with 3 mL of RPMI-1640 per and allowed to incubate for 24 hours at 37°C. Cells were treated with various drugs as indicated with an incubation time of 24 hours. 48 hours after initial seeding, cells were trypsinized, collected, and counted for a density of approximately  $1 \times 10^6$ /mL per sample. FCCP was used as a positive control (20 $\mu$ M) and incubated for 15 minutes at 37°C prior to staining. All samples were then stained at 200nM per sample with either TMRE reagent (Cayman chemical # 701310) or JC-1 reagent (MedChemExpress # HY-15534) and incubated at 37°C for 30 minutes. Cells were centrifuged at 2,000rpm for 3 minutes and resuspended in 300 $\mu$ L fresh 1XPBS for analysis. Samples were analyzed using BD FACSymphony A5 Cell analyzer and FlowJo software.

### **2.3.7 RNA Sequencing Analysis**

LNCaP, MR49F, C4-2, and C4-2R cells were previously treated with varying drug combinations for 48 hours prior to total RNA extraction. Extraction was achieved using Qiagen's RNeasy Mini Kit (#74104) according to the manufacturer's instructions. All samples were sent to Novogene Biotechnology Company (Ca, USA) for RNA quality assessment, library construction, Illumina sequencing, and data analysis. DEseq2 R package was used to analyze gene expression data normalization and differential expression. Significantly up/down regulated genes were determined as a fold change of  $\geq 2$  and q value of  $< 0.05$ .

### **2.3.8 22Rv1-derived Xenograft Mouse Model**

All animal experiments were approved by the Institutional Animal Care and Use Committee (IACUC) at the University of Kentucky. 22Rv1 cells were mixed with equal volume of Matrigel and inoculated subcutaneously at  $2.5 \times 10^6$  cells/mouse into the right flank of pre-castrated nude mice. After a week following inoculation, mice were randomized into four treatment groups. Enzalutamide (30mg/kg) was dissolved in 10% dimethyl sulfoxide (DMSO) and 90% corn oil and Metformin HCl (20mg/kg) was dissolved in sterile water and administered through oral gavage daily for 4 weeks. Tumors were measured every 3 days and tumor volume was estimated using the following formula  $V = L \times W^2/2$  where  $V$  is volume in cubic millimeters,  $L$  is length in millimeters, and  $W$  is for width in millimeters.

### **2.3.9 LuCaP35CR Xenograft Mouse Model**

NOD scid gamma (NSG) mice bearing LuCaP35CR tumors were obtained by Dr. Robert Vessella at the University of Washington. For tumor amplification, tumor sections were harvested and implanted subcutaneously into the flanks of pre-castrated NSG mice. When tumors reached a large size, tumors were harvested and sectioned into approximately  $25\text{mm}^3$  pieces. Tumor pieces were implanted into 40 pre-castrated NSG mice. Once the tumors reached approximately  $200\text{mm}^3$ , mice were randomized into 4 treatment groups. Enzalutamide (30mg/kg) was dissolved in 10% dimethyl sulfoxide (DMSO) and 90% corn oil and Metformin HCl (20mg/kg) was dissolved in sterile water and administered through oral gavage daily for 4 weeks. Tumors were measured every 3 days and tumor volume was

estimated using the following formula  $V = L \times W^2/2$  where  $V$  is volume in cubic millimeters,  $L$  is length in millimeters, and  $W$  is for width in millimeters.

### **2.3.10 Histology and Immunohistochemistry**

Xenograft tumors were fixed in 10% neutral-buffered formalin with rocking overnight and transferred into 70% ethanol the following day. Tumors were paraffin embedded, sectioned to 5mM sections, mounted, and processed using conventional hematoxylin and eosin (H&E) staining. Sections were also stained for the Ki67 proliferation marker and cleaved caspase 3.

### **2.3.11 Statistical Analysis**

Numerical data is represented as mean  $\pm$  SD. Statistical significance of the results was analyzed by using unpaired two-tailed t test. The p values of  $<0.05$  indicates statistical significance.

## **2.4 Results**

### **2.4.1 Metformin treatment exhibits a synergistic effect with enzalutamide in ENZ-r CRPC lines.**

To determine the optimal doses of either enzalutamide or metformin for the attenuation of prostate cancer growth *in vitro*, we first utilized a cell viability assay and calculated IC<sub>50</sub> values. For both isogenic lines, the enzalutamide sensitive IC<sub>50</sub>s of enzalutamide were lower than their enzalutamide resistant counterparts where LNCaP and C4-2 IC<sub>50</sub> values were 14.5mM and 22.mM respectively, MR49F and C4-2R IC<sub>50</sub> values were 26mM and 35mM respectively (**Fig 2.1A,C**) which were consistent with our previous findings [109]. The IC<sub>50</sub> value for enzalutamide-treated 22Rv1 cells was 110mM (**Fig 2.1E**). The same strategy was

applied to measure the IC<sub>50</sub> values of metformin where LNCaP was 2.1mM, MR49F was 3.2mM, C4-2 was 4.1mM, C4-2R was 1.7mM, and 22Rv1 was 15.4mM (**Fig 2.1B,D,F**). Utilizing these doses, we sought to test whether metformin would enhance enzalutamide inhibition of cell growth using a clonogenic assay. All three ENZ-r lines were seeded at a low density and treated with DMSO as a control, 10mM, 20mM, or 30mM of enzalutamide for MR49F, C4-2R, or 22Rv1 respectively, 1mM of metformin alone or in combination with enzalutamide for 14 days followed by crystal violet stain (**Fig 2.1G-I**). From the quantification, all three ENZ-r lines exhibited varying decreases in cell growth in mono treatment. However, combination treatment exhibited the greatest significant cell growth attenuation ( $p \leq 0.001$ ). To test whether metformin synergizes with enzalutamide to inhibit cell proliferation, we utilized a cell viability assay. Cells were treated with increasing combinations of enzalutamide or metformin and analyzed using the highest single agent (HSA) synergy model. We observed a strong synergistic effect in ENZ-r cells treated with a minimum of 1mM metformin in combination with enzalutamide (**Fig 2.1J-L**). Together, these results suggest that enzalutamide and metformin have a synergistic effect on drug resistant prostate cancer growth *in vitro*.

#### **2.4.2 Combination treatment results in metabolic reprogramming**

Previous studies demonstrated the reliance of OX PHOS in advanced PCa [5]. We hypothesized that utilizing metformin in combination with enzalutamide would subject the prostate cancer cells to an energy crisis and vulnerability to apoptosis. To gain a better understanding of the effect of combination treatment on

mitochondrial function, we treated ENZ-r cells followed by a mitochondrial stress test via seahorse analysis. We utilized the mitochondrial stress test to directly measure the oxygen consumption rate of cells (OCR) following injection of key modulators of cellular respiration to determine mitochondrial function [110, 111]. In MR49F cells, combination treatment lowered basal respiration, proton leak, ATP production, and spare respiratory capacity indicating an overall decline OXPHOS (**Fig 2.2A-C**). Similarly, we confirmed these findings in C4-2R cells where the basal respiration, proton leak, and ATP production was decreased compared to control cells, however, C4-2R cells were markedly more sensitive to metformin treatment as the overall oxygen consumption rate (OCR) was much lower compared to MR49F (**Fig 2.2D-F**). Interestingly, combination treated C4-2R cells exhibited a higher spare respiratory capacity than metformin treatment alone indicating an increased capability of the cell to respond to energetic demand. Next, we sought to measure the mitochondrial membrane potential (MMP) in response to combination treatment as an indicator of ATP production [112]. As the MMP depolarizes, the membrane will become more permeable allowing protons to diffuse out of the intermembrane space. Disruption of the proton gradient will inhibit ATP synthase resulting in an overall inhibition of OXPHOS. We utilized TMRE, a fluorescent chemical indicating metabolic fitness, to stain ENZ-r cells following combination treatment followed by flow cytometric analysis. FCCP, an ETC uncoupler, was used as a positive control for near complete depolarization of the MMP. All samples were normalized to FCCP where TMRE- cells are indicative of MMP depolarization. In both MR49F and 22Rv1 cells, we did not observe any

difference in MMP depolarization 24 hours after treatment (**Fig 2.2G,I**). Interestingly, we observed an increase in TMRE fluorescence in combination treatment compared to control which indicates an overall increased metabolic fitness (**Fig 2.2H**). These data are consistent with our results from the mitochondrial stress test, in that C4-2R cells seem to exhibit increased mitochondrial function in response to combination treatment. Finally, to confirm our results from TMRE, we employed a similar method of measuring MMP with the JC-1 chemical which is considered more sensitive than TMRE. JC-1 differs from TMRE in that upon entrance into the mitochondria, the aggregate will emit a red color, indicative of a polarized and metabolically energetic MMP. Following depolarization of the MMP, JC-1 will present as monomers and diffuse out of the intermembrane space, emitting a green color. After flow cytometric analysis, we observed a similar ratio of red/green% cells between control, enzalutamide and combination in MR49F cells with Metformin solo treatment having the greatest effect at depolarization of the MMP (**Fig 2.2J**). In C4-2R cells, metformin mono treatment and combination treatment remain similar to control in MMP. Due to the large error bar of the C4-2R enzalutamide mono treatment, further replicates need to be performed to generate conclusive data. 22Rv1 cells exhibited a similar effect on MMP across all treatment groups. Together, this data suggests that combination treatment may have a small effect on metabolic fitness of the mitochondria, however, conclusive evidence is lacking at this time.

### **2.4.3 Combination treatment effect on 22Rv1-derived xenograft tumors**

To investigate our findings in vitro, we evaluated the effect of enzalutamide and metformin alone or in combination with a 22Rv1-derived xenograft mouse model. 22Rv1 cells express the AR-V7 splice variant of AR which harbors a truncated form of the ligand binding domain (LBD) and preventing enzalutamide binding, making these cells intrinsically resistant to enzalutamide [40]. Following 50 days of treatment, metformin alone exhibited a similar rate of tumor growth as control while enzalutamide alone and combination treatment groups had similar rates to each other (**Fig 2.3A**). Similarly, the tumor weights for all 3 treatment groups after harvest were not significantly decreased compared to control, however, enzalutamide on its own did exhibit a decreasing trend (**Fig 2.3B**). Images from the harvested tumors confirm our results ultimately observing no significant changes in tumor size compared between groups (**Fig 2.3C**). There was no observable difference in body weight between groups indicating a lack of treatment toxicity (**Fig 2.3D**). Following harvest, we processed the tumors for IHC analysis. H&E staining of tumor samples visually indicated a slight decrease in tumor cell number in combination treatments, although enzalutamide mono treatment may have had the greatest effect (**Fig 2.3E**). To measure proliferation, we stained IHC samples with proliferation marker Ki67 and observed what appears to be a general decrease in proliferation in combination treated tumors, however, further analysis and confirmation by a pathologist would be required to make such claim (**Fig 2.3F**). Finally, cleaved caspase-3 staining of tumor samples indicated a similar level of apoptosis across samples, although further studies will be required to confirm

these results (**Fig 2.3G**). Interestingly, despite observation of an inhibition of prostate cancer cell growth *in vitro*, we did not observe the same effects on PCa growth *in vivo* following combination treatment.

#### **2.4.4 Combination treatment effect on LuCaP35CR xenograft tumors**

To further investigate the results of our *in vitro* work, we also employed a LuCaP35CR xenograft model, which is more closely related to patient samples, to determine the effect of combination treatment on tumor growth. Consistent with our previous results in the 22Rv1-derived xenograft experiment, LuCaP35CR did not exhibit any significant changes in tumor volume within the 4 treatment groups 50 days following initial treatment (**Fig 2.4A**). Immediately upon harvest tumors were weighed and exhibited no significant changes between treatment group tumors (**Fig 2.4B**) or between tumor size indicated by the tumor images in **Figure 2.4C**. To determine toxicity, we measured body weight in the 4 groups throughout the study and while there may be an observable difference between treatment groups and control, this could be due to the small sample size for all groups (n=5) (**Fig 2.4 D**). Taken together, our *in vivo* results indicate a lack of synergistic effect *in vivo*, in contrast to the phenotype we observed *in vitro*.

#### **2.4.5 RNA Sequencing analysis of isogenic ENZ-r CRPC lines.**

To determine the mechanism in which CRPC lines respond to combination treatment, we performed RNA sequencing analysis with the isogenic sensitive and ENZ-r lines listed previously. After enzalutamide or metformin mono treatment or in combination, we compared gene lists to determine differences in RNA expression in for genes that were specific to ENZ-r combination treated samples

(**Fig 2.5A**). C4-2R combination treated gene sets exhibit a significant decrease in genes in the Ras signaling pathway as well as phospholipase D signaling and genes related to the lipid and atherosclerosis pathway (**Fig 2.5B**). Based on these results, we can speculate that a downregulation in Ras signaling specifically would inhibit cell growth and proliferation [113]. In addition, phospholipase D signaling as well as lipid and atherosclerosis signaling play roles in cellular metabolism as well as cross signaling with traditional oncogenic signaling pathways such as Ras, mTOR, and MAPK signaling, and we observe their downregulation in our samples [113-116]. We observed similar results in the significant down regulation of genes associated with the MAPK signaling, lipid and atherosclerosis pathways and calcium signaling. As with C4-2R cells, these down regulated pathways foreshadow a shift in gene expression towards the inhibition of cell proliferation and cellular metabolism pathways (**Fig 2.5D**). In contrast, we observe an up-regulation of both cell cycle signaling proteins as well as proteins related to various DNA repair pathways in both C4-2R (**Fig 2.5C**) and MR49F (**Fig 2.5E**) following combination treatment. It is currently unclear how the upregulation of these genes may influence these ENZ-r prostate cancer cells; further analysis is required to investigate these results.

## **2.5 Discussion**

While treatments and therapies continue in development for various cancers at different stages, drug resistance remains a serious issue in advanced CRPC and identifying novel treatment strategies is critical [117, 118]. Enzalutamide, as a competitive inhibitor of AR signaling, continues to be the only FDA-approved

therapy for metastatic CRPC, however, resistance to treatment often occurs. In this study, we assessed whether combination treatment of enzalutamide and metformin in enzalutamide-resistant prostate cancer lines would induce an energy crisis and therefore induce vulnerability to apoptosis [29]. Our results demonstrate that the combination treatment is synergistically compatible to inhibit drug resistant prostate cancer growth *in vitro*. Cell proliferation in ENZ-r was significantly inhibited following combination treatment (**Fig 2.1G-I**) and our results indicate that the two drugs tested act synergistically together using an HSA synergy model (**Fig 2.1J-L**) [119]. These results suggest a vulnerability in the metabolic signaling of ENZ-r PCa cells which may have allowed for exploitation and ultimately cell death with enzalutamide treatment.

While our combination treatment exhibited a similar growth inhibition phenotype across all 3 ENZ-r lines, we observed differences in mitochondrial function between these lines. It has been well documented that the mitochondrial stress test is a robust method in testing mitochondrial function [111]. After combination treatment, MR49F cells exhibited more of a lack in mitochondrial function indicated by an overall lower basal consumption rate, lower spare respiratory capacity, and decreased ATP production (**Fig 2.2A-C**). In contrast, combination-treated C4-2R cells responded similarly to metformin mono treatment with a decreased basal respiration rate and ATP production, however, combination treatment may have a better capacity to respond to metabolic stress indicated by a higher respiratory capacity (**Fig 2.2D-F**). The observed difference in mitochondrial respiration between these two cell lines may be a result of the

differences in metabolic gene expression. In addition, utilizing an acute injection mitochondrial stress test and measuring the changes in OCR immediately following treatment may yield interesting changes in respiration as this experiment would capture the immediate responses to treatment. The mitochondrial membrane potential is maintained by the electron transport chain as a means of producing a proton gradient for ATP synthase to function, therefore, depolarization of the MMP is indicative of OX PHOS inhibition [112]. While we tested two different means in which the MMP can be measured for all 3 ENZ-r lines, we did not observe a significant difference in polarization between treatment groups compared to control (**Fig 2.2G-J**). While the MMP is indicative of OX PHOS inhibition, the MMP can stabilize quickly following challenge and may be best observed in an acute treatment experiment. To better observe the metabolic shift from OX PHOS to glycolysis, the glycolytic rate assay could be employed as a rigorous method in which rapid metabolic switches can be detected [120]. In addition, determining mitochondrial mass following treatment may be another method to measure the mitochondrial response of either fission or fusion [121].

While our *in vitro* results demonstrate a synergistic effect on PCa growth, the same effect was not observed in either 22Rv1-derived xenograft model (**Fig 3**) or in the LuCaP35-CR xenograft model (**Fig 4**). One potential reason for the significant difference between 22Rv1-derived xenograft response to combination treatment and the observable phenotype *in vitro* is the difference in the metabolic profile for 22Rv1 cells. As we observed with the MMP, 22Rv1 cells did not exhibit a difference between treatment groups, indicating that the ATP synthase remained

functional due to the stable polarization of the mitochondrial membrane (**Fig 2.2I**). 22Rv1 cells are typically used as the standard xenograft model in testing drug-resistant CRPC as they are intrinsically resistant to enzalutamide and account for the AR-V7 [122, 123], however, we observed that C4-2R and MR49F cells were more sensitive to changes in metabolism than 22Rv1 cells (**Fig 2.2 A-H**). Another potential explanation for the difference in responses to combination treatment between *in vitro* and *in vivo* models could be the route of administration and treatment. In our study, we used an oral gavage technique with treatments at the concentrations listed in the methods section, however, utilization of an intraperitoneal (IP) technique might have yielded better results in the mice as this is a method of direct administration [124]. In addition to changes in administration, metformin may be more sensitive to freeze/thaw than we anticipated. Future treatments with metformin *in vivo* may require dissolving smaller doses for treatment to avoid freeze/thawing effects.

In summary, the present study demonstrates the difficulty in treating drug resistant CRPC as the combination treatment of enzalutamide and metformin *in vitro* demonstrated a positive attenuation of PCa growth, however, this effect was not observed *in vivo*. Our results highlight the importance of investigating different treatment in robust *in vitro* and *in vivo* models. Despite drug-resistant CRPC's reliance on OX PHOS in energy metabolism, inhibition of OX PHOS with metformin did not produce an observable phenotype on ENZ-r lines.

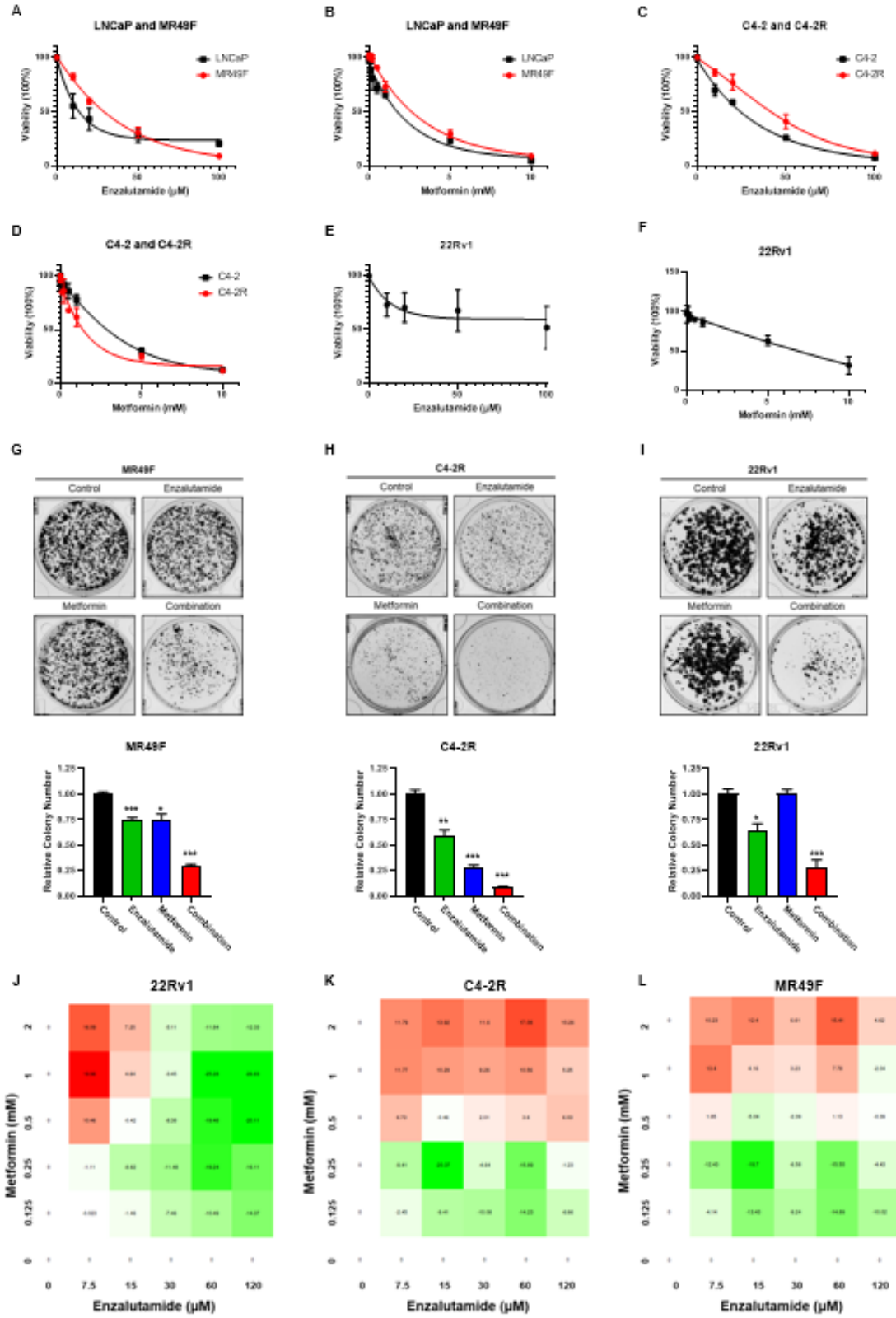


**Figure 2.1 Enzalutamide and Metformin in combination synergistically inhibit growth of enzalutamide resistant CRPC *in vitro*.**

Cell viability assay of isogenic CRPC lines treated with either enzalutamide (**A, C, E**) or metformin (**B, D, F**) to compare IC<sub>50</sub> values. Data is scaled into percentage and normalized to untreated groups, then shown as mean ±SD (n=3). Clonogenic assay of MR49F (**G**), C4-2R (**H**), and 22Rv1 (**I**) treated with DMSO as control or drugs indicated for up to 14 days. Quantification of relative colony number are indicated below where \*, p ≤ 0.05; \*\*, p ≤ 0.01; \*\*\*, p ≤ 0.001. Synergy scores were calculated for MR49F (**J**), C4-2R (**K**), and 22Rv1 (**L**) after treatment with varying doses of the indicated drugs. Scores ≤ -10 indicate an antagonistic interaction, scores between -10 and 10 indicate an additive effect, and scores ≥ 10 are considered synergistic.

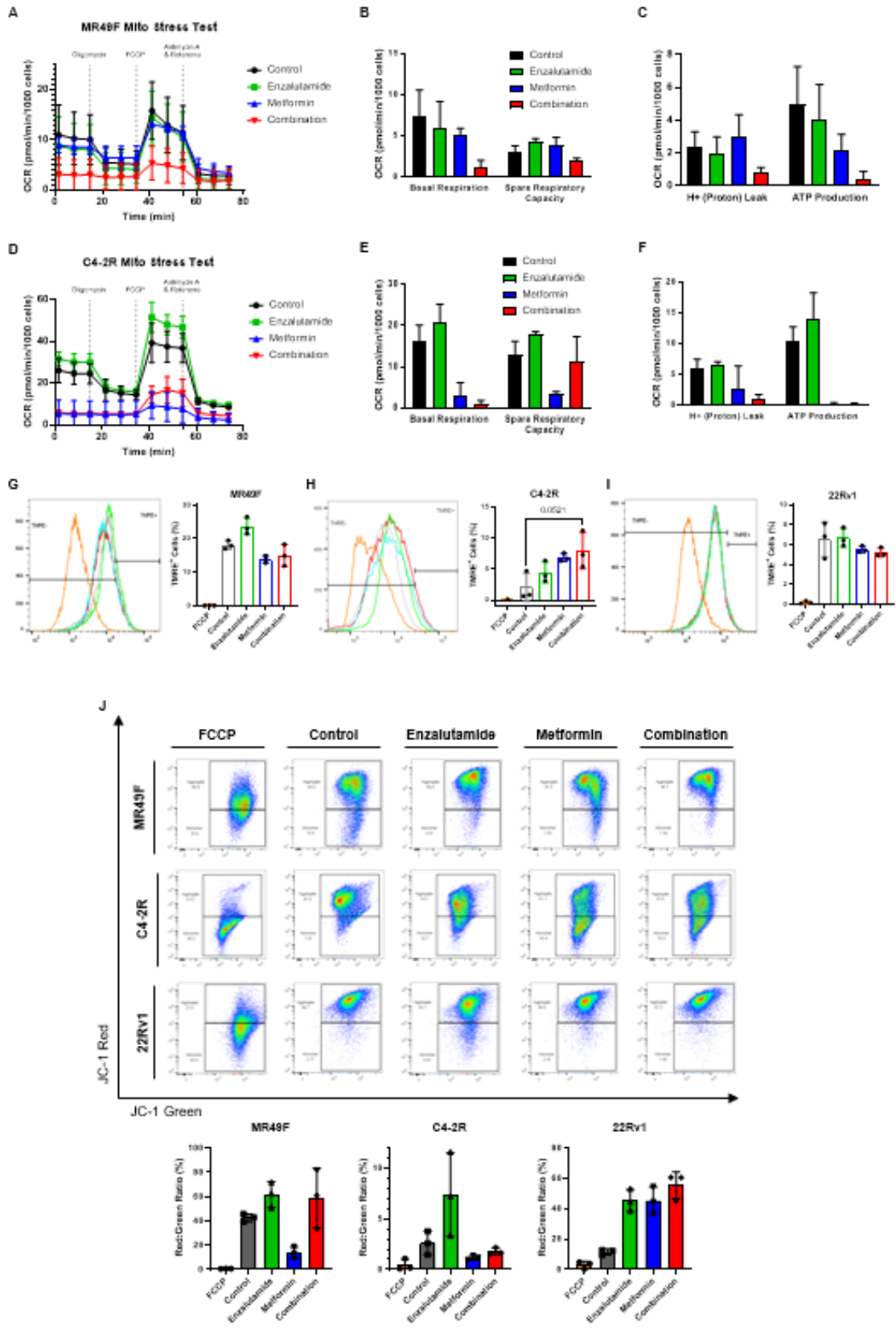


## **Figure 2.2 Combination treatment results in metabolic reprogramming.**

Representative traces of the oxygen consumption rate (OCR), when oligomycin, carbonyl cyanide-4-(trifluoromethoxy) phenylhydrazone (FCCP), antimycin A plus rotenone were injected into the assay XF96 plates for MR49F **(A-C)** and C4-2R **(D-F)** cells. Each data point is a mean  $\pm$  standard deviation (n=6). Cells were treated with or without 10 $\mu$ M enzalutamide, 1mM metformin, or a combination of both for 12 hours. Mitochondrial membrane potential was measured using tetramethylrhodamine, ethyl ester, perchlorate (TMRE). MR49F **(G)**, C4-2R **(H)**, and 22Rv1 **(I)** cells were treated with or without enzalutamide, metformin, or a combination of both for 12 hours and collected for flow cytometric analysis. FCCP was used as a positive control. **(J)** The mitochondrial membrane potential was measured with the same treatment as with TMRE in all 3 resistant lines, but the chemical JC-1 was used to visualize the membrane potential shift.

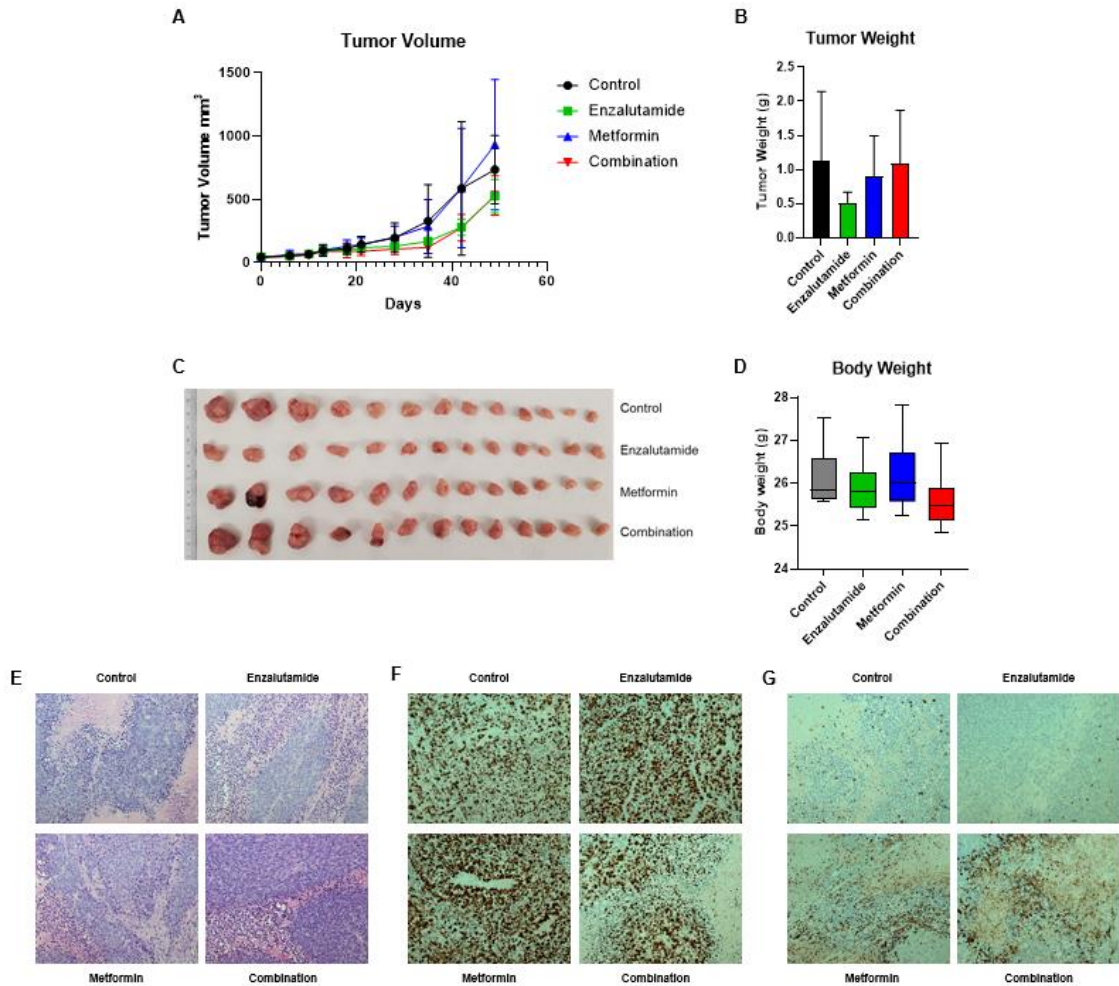


**Figure 2.3 Combination treatment of enzalutamide and metformin did not attenuate 22Rv1 Xenograft tumor growth *in vivo*.**

**(A)** Tumor growth curves of 22Rv1-derived xenograft. After pre-castrated nude mice were inoculated subcutaneously with 22Rv1 cells ( $2.5 \times 10^6$ /mouse) and allowed to grow for 2 weeks. After 2 weeks, the mice were treated with various drugs as described in the methods section of this chapter. The sizes of the tumors in each group were measured every 3 days (mean  $\pm$  SD; n= 13 mice per group). **(B)** Measurement of tumor weight immediately after harvest. **(C)** Images of 22Rv1-derived tumors at the end of the study. **(D)** Measurement of mouse body weight

throughout the study. **(E)** Representative images of H&E staining on formaldehyde-fixed, paraffin-embedded, 22Rv1-derived tumor sections. **(F)** Representative images of anti-Ki67 IHC staining of tumor sections. **(G)** Representative images of anti-cleaved caspase-3 IHC staining of tumor sections.

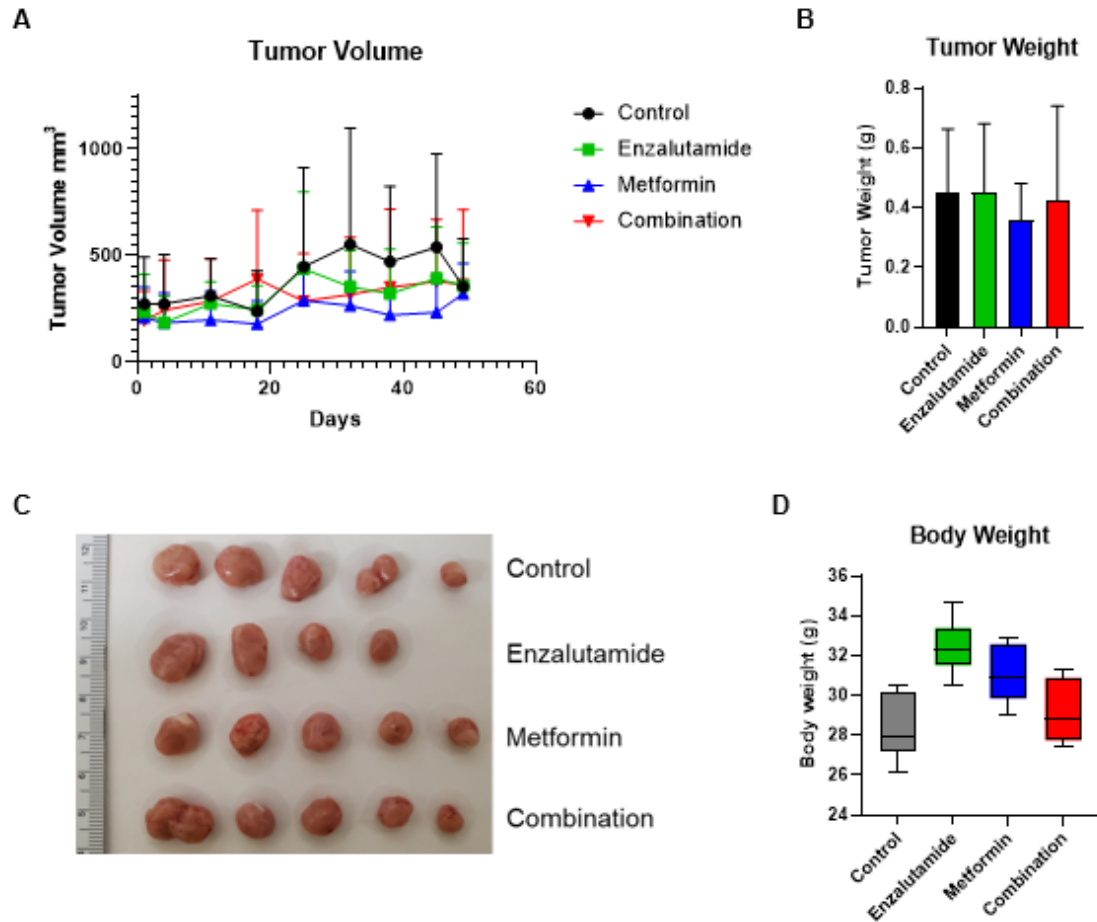


**Figure 2.4 Combination treatment of enzalutamide and metformin did not attenuate LuCaP35CR tumor growth *in vivo*.**

**(A)** Tumor growth curves of LuCaP35CR xenografts (mean  $\pm$  SD; n= 4 mice per group). **(B)** Measurement of tumor weight immediately after harvest. **(C)** Images of LuCaP35CR tumors at the end of the study. **(D)** Measurement of mouse body weight throughout the study.

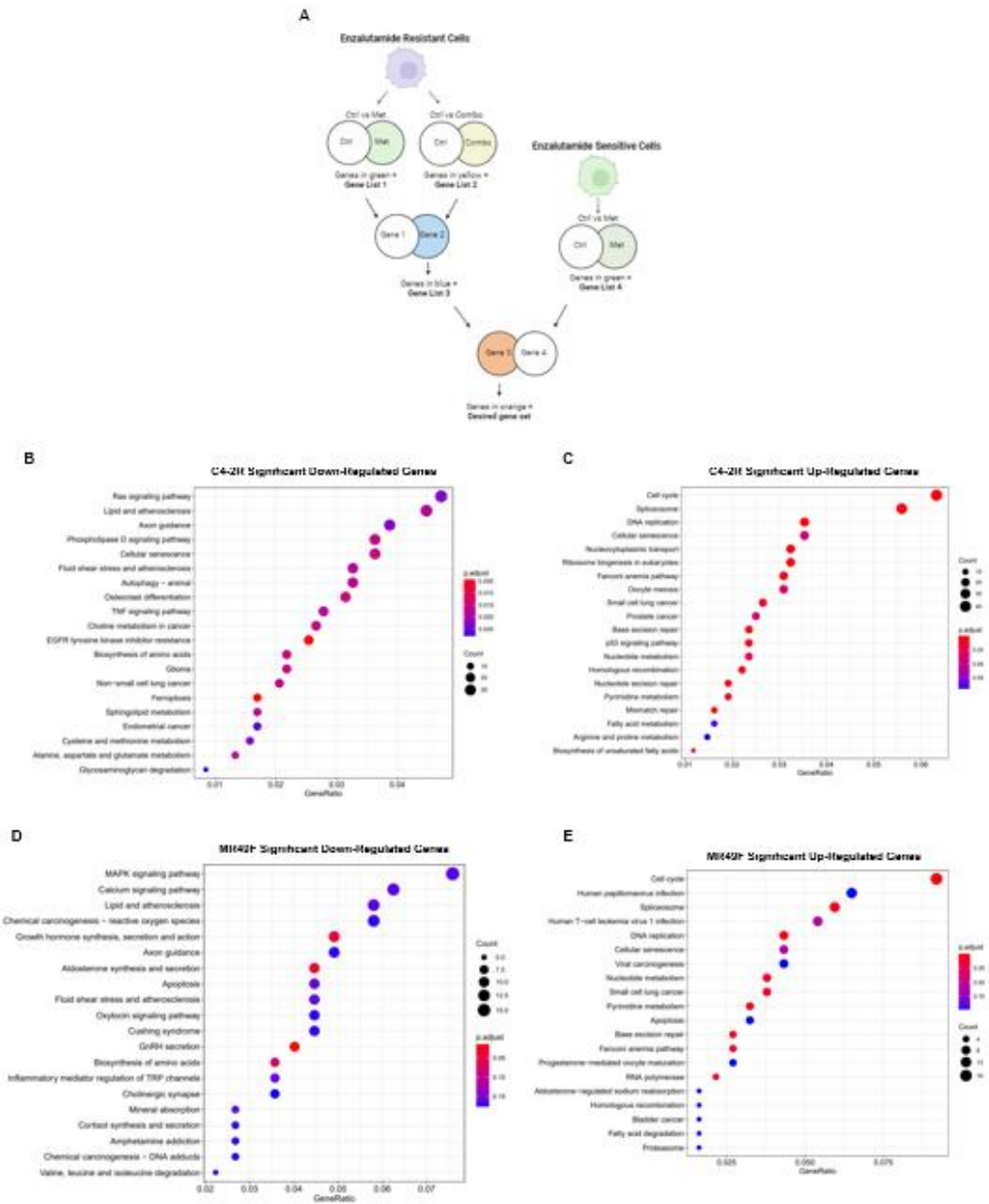


**Figure 2.5 RNA sequencing analysis of isogenic CRPC lines.**

**(A)** Schematic representation of gene comparisons for RNA sequencing result analysis. Dot plot analysis of significant C4-2R downregulated **(B)**, upregulated **(C)**, MR49F downregulated **(D)**, and upregulated **(E)** pathways.

## CHAPTER 3. The regulation of Mre11a via Plk1 phosphorylation in thymic lymphoma

### 3.1 Overview

Genomic stability remains one of the crucial cellular characteristics that prevent carcinogenesis, since an accumulation of DNA damage is a hallmark of various cancers. To maintain homeostasis, cells must retain the ability to prevent mutation accumulation; this occurs via the DNA damage response (DDR), which targets the site of DNA damage and recruits downstream effector proteins that either resolves the damage or induces apoptosis. Within the DDR for double strand breaks (DSB), critical proteins such as those in the Mre11a-Rad50-NBS1 (MRN) complex are crucial to complete this type of repair. Specifically, Mre11a, as part of the MRN complex, will resect the damaged DNA and create 3' overhangs to promote Rad51 strand invasion [125]. DNA end resection primarily during homologous recombination (HR). Evidence has shown that tight regulation of the DDR during this period of vulnerability is critical for cell survival.

Our lab has demonstrated that polo-like kinase 1 (PLK1), together with casein kinase 2 (CK2), phosphorylate Mre11a during G2 DNA damage checkpoint recovery to prematurely terminate the DDR signaling pathway and therefore inhibit DNA repair observed during irradiation (IR) associated carcinogenesis. While PLK1 is well known for its roles in mitotic regulation, the implication of regulation in the DDR pathway led our lab to generate a knock-in genetically engineered mouse (GEM) model of Mre11a which harbors two point mutations which mimic phosphorylation by PLK1 and CK2 (Mre11a<sup>S648Dand S686D</sup>). In this study, we utilized

an *in vivo* radiation-induced carcinogenesis model to investigate the effects of the constitutively active phospho-mimic form of Mre11 on DNA damage accumulation. While we initially observed a rescue phenotype of Mre11a<sup>SSDD</sup> in the delay/prevention of radiation-induced carcinogenesis, this result was not consistent for the rest of the study. Similarly, a medium-high single dose of IR had no effect on the delay or induction of carcinogenesis *in vivo*. Similarly, utilizing a lethal dose of IR, we observed no differences in survival between WT and Mre11a<sup>SSDD</sup> mice. After harvesting mouse embryonic fibroblasts (MEFs) from our knock-in mouse model, we tested the effects of IR on cell viability, and again saw no effect. In contrast, when we tested  $\gamma$ H<sub>2</sub>AX induction immediately following IR, we see a slight extension of  $\gamma$ H<sub>2</sub>AX in the Mre11a<sup>SSDD</sup> MEFs via immunoblotting which was confirmed via immunofluorescence.

### **3.2 Introduction**

It is well known that IR induces damaging effects on exposed cells in both pathways and damage levels. Particularly, cells exposed to IR, a carcinogen, will accumulate clusters of DNA damage ranging between double strand breaks (DSB) and single strand breaks (SSB) often leading to oncogenic mutations that initiate/promote tumorigenesis [91]. On the contrary, IR is a powerful tool used to treat primary cancers, however, exposure to such treatments can promote secondary cancers and other debilitating side effects [126]. Historically, to study the risk factors and mechanisms of radiation-induced carcinogenesis, a split low dose treatment scheme of radiation has been utilized as a reliable method for the induction of thymic lymphoma [92, 93, 127]. Due to the nature of the hematopoietic

system, enduring constant renewal through the life of the individual, it has a specific vulnerability to either inherited or acquired genetic diseases [128, 129]. Split low dose radiation exposure is uniquely designed to induce mutational burden in a model that can easily be monitored by immature T cell formation. Normally, immature T cells presenting both CD4 and CD8a are found only in the thymus where they mature before entering the blood stream. However, in the case of thymic lymphoma, immature CD4+/CD8a+ double positive T cells can be found in circulation [95]. As DNA repair functions to prevent mutation accumulation and therefore plays a crucial role in genomic stability, we used this model to understand how manipulation of the DNA damage response (DDR) pathway might alter initiation and progression of carcinogenesis.

Maintaining the genomic integrity of an organism is critical for continued life, therefore, mechanisms in which the organism can repair continual challenges is crucial. In general, the DDR comprises a signaling cascade which includes the recruitment of the MRN complex, activation of ATM/ATR, and the induction of  $\gamma$ H<sub>2</sub>AX [67]. DNA lesions are first sensed by the MRN complex followed by the activation of ATM/ATR triggering downstream DDR [71]. Within the DDR for DSB, non-homologous end joining (NHEJ) and homologous recombination (HR) are the two primary methods of repair, both of which rely on the nuclease activities of Mre11a [73]. Mre11a possess both endo- and exonuclease activity against both single strand breaks and DSBs and is therefore crucial for the DSB DDR.

In recent years, it has been suggested that polo-like kinase 1 (PLK1), an essential mitotic regulation kinase, may also play roles in the regulation of cellular

processes outside of cell cycle such as epigenetics and DNA damage repair [130-132]. Particularly, evidence suggests that PLK1 is also involved in many DDR events such as G2 DNA damage check point recovery [133]. In addition, PLK1 has been demonstrated as a critical component in the degradation of ATR-mediator claspin [134], inactivation of Chk2 signaling via phosphorylation of 53BP1 [135], as well as phosphorylation of upstream DDR proteins such as Mre11a for premature checkpoint termination in G2 DNA damage recovery [89]. Collectively, these studies highlight the important role that PLK1 plays in the DNA damage response, however, the functions of PLK1 in these pathways remain to be elucidated. In this study, we utilize a GEM double mutant knock-in model of Mre11a recapitulating phospho-mimic mutation phosphorylation sites for PLK1 and CK2 respectively to determine the effect of radiation-induced carcinogenesis *in vivo*.

### **3.3 Materials and Methods**

#### **3.3.1 Mouse Lines and Genotyping**

Animal experiments in this study were approved by the Institutional Animal Care and Use Committee (IACUC) at the University of Kentucky. *Mre11a*<sup>S648DandS686D</sup> conditional double mutation knock-in mice (*Mre11a*<sup>SSDD</sup>) were generated by Taconic Labs. Briefly, the NCBI transcript NM\_018736.3 for Mre11a was used. The 3' part of intron 17 containing the splice acceptor site and fused exons 18 to 20 including the 3' untranslated region (UTR) were flanked by loxP sites inserted into intron 17. An additional human Growth Hormone polyadenylation signal (hGHpA) was inserted between the 3' UTR and the distal

loxP site to prevent downstream transcription of the mutated exons 18 and 19. Mutations were introduced into exons 18 and 19 respectively downstream of the distal loxP site. Positive selection markers, flanked by FRT sites (neomycin resistance: NeoR) and F3 (Puromycin resistance: PuroR), were inserted downstream of the proximal loxP site and upstream of the distal loxP site. The targeting vector was generated using bacterial artificial chromosomes (BAC) clones from the C57BL/6J RPCI-23 BAC library and was transfected into the Taconic Biosciences C57BL/6N Tac ES cell line. To determine the genotype of WT or *Mre11a*<sup>SSDD</sup> mice, DNA was extracted from ear snips using the standard Jackson laboratory alkaline lysis buffers. PCR sense (5'-AAGCACTGACAGTCTGTTGCC-3') and antisense (5'-TCCGTTTGCTAGATGTTGTGC-3') primers were used to detect the conditional knock-in allele of *Mre11a*<sup>SSDD</sup>. Control PCR sense (5'-GGGGCAATCAATTGAGGG-3') and antisense (5'-CAACCTCTGCTTGGTTCTGG-3') primers were used to detect the wildtype CD79b gene and determine successful cycling. To determine *Mre11a* zygosity, PCR sense (5'-GTGTATTTTAGAGGCTACAGCTTGC-3') and PCR antisense (5'-ACCTCAATGGTCTACAGAAGGG-3') primers were used to detect the *Ndufb7* wildtype gene. Crossing of *Mre11a*<sup>SSDD</sup> with *Rosa26-CreERT2* (B6.129, Jackson Laboratory Stock No. 008463) produced *Mre11a*<sup>SSDD</sup>;*Rosa26-CreERT2* mice. To genotype *Rosa26-CreERT2* mice, PCR sense (5'-GCGGTCTGGCAGTAAAACTATC-3') and PCR antisense (5'-GTGAAACAGCATTGCTGTCACTT-3') primers were used.

### **3.3.2 Tamoxifen Treatment and Total Body Irradiation (TBI)**

6-8 week old adult *Mre11a*<sup>SSDD</sup>;*Rosa26-CreERT2* mice were dosed via oral gavage with either tamoxifen dissolved in corn oil, or corn oil alone as vehicle control, at 75mg/kg daily for 5 days to induce *Mre11a* double mutation knock-in. To achieve total body irradiation (TBI), mice were anesthetized via ketamine:xylazine:saline (k/x) solution in a ratio of 0.1:0.05:0.85 7 days after induction. Solutions were injected intraperitoneally (IP) and the volume of injection was calculated as a ratio of 150µL per 19g body weight. Anesthetized mice were placed in the chamber of the X-Rad160 (Precision X-Ray Irradiation) X-Ray irradiator. The dose rate for exposure was 86.6cGy/min but specific exposures are given when describing experiments. Solutions of 30X revertidine were injected IP following irradiation at the same volume of injection as the k/x solution per mouse. Mice were monitored daily for 10 days following irradiation.

### **3.3.3 Flow Cytometric Analysis**

Single cell suspensions of bone marrow, thymus, spleen, and peripheral blood were prepared and stained with flouochrome-conjugated antibodies: CD4 (APC-Cy7), CD8a (FITC), CD3 (PE), CD45.1 (Pacific Blue). Data was acquired using BD FACSymphony A5 SE cell analyzer (BD Biosciences) using FACSDiva software and analyzed with FlowJo version 10 analysis (Tree Star). Samples were suspended in FACS buffer of 1X PBS and cell doublets were excluded from analysis.

### **3.3.4 Complete Blood Count**

Complete blood count was achieved using 20 $\mu$ L of whole blood collected in heprin coated capillary tubes and subjected to measurement using a Hemavet 950 (Drew Scientific).

### **3.3.5 Histological and Immunohistochemical (IHC) Analysis**

Mouse tissues were removed surgically, kept on ice, washed in ice-cold 1X PBS, fixed in 10% neutral-buffered formalin during overnight rocking, and transferred into 70% ethanol the following day. Tissues were paraffin embedded, sectioned to 5mM sections, mounted, and stained using the conventional hematoxylin and eosin (H&E) staining. Sections were also stained for the Ki67 proliferation marker, CD45.1, CD3, CD8a, and CD4.

### **3.3.6 Establishment of Mouse Embryonic Fibroblasts (MEFs)**

Day 13.5 embryos were harvested from an adult female *Mre11a<sup>SSDD</sup>;Rosa26-CreERT2* mouse, and the heads and organs were removed. Tissue was minced and rinsed with 1X PBS followed by digestion with 0.1% trypsin containing EDTA for 10 minutes at 37°C. Trypsin was inactivated by DMEM supplemented with 10% FBS and cells were plated onto a 10cm dish. The medium was changed 24 hours following plating to remove large tissue clumps. To induce conditional knock-in of the *Mre11a* double mutation, MEFs were treated with 1 $\mu$ M tamoxifen for 48 hours prior to experimentation. The genotypes of the embryos were detected by PCR with the primers listed above. Cells were cultured at 37°C with 5% CO<sub>2</sub> in DMEM supplements with 10% FBS and 1% penicillin/streptomycin.

MEFs were frozen at passage 1, stored in liquid nitrogen, and thawed for use in subsequent studies.

### ***3.3.7 Immunoblotting***

MEFs, either exposed to tamoxifen or isopropanol as vehicle control, were previously treated with varying exposures of irradiation and at varying times before harvest at times indicated in each experiment. Cell lysis was achieved using 10% RIPA solution with protease and phosphatase inhibitors followed by sonication. Protein concentration were measured by Pierce BCA Assay kit and equal concentrations of protein lysate from each sample were mixed with SDS loading buffer, resolved using SDS-Page gel electrophoresis, and transferred to either Nitrocellulose or PVDF membranes followed by blocking and incubation with primary and HRP-conjugated secondary antibodies. ECL was used to induce chemiluminescence and membranes were imaged using BioRad ChemiDoc MP. BioRad ImageLab software was utilized to analyze immunoblots.

### ***3.3.8 Immunofluorescence***

MEFs, either exposed to tamoxifen or isopropanol as vehicle control, were previously treated with 3Gy total irradiation and fixed at varying time points with 10% neutral-buffered formalin following 3 washes with 1X PBS. Following fixation, permeabilization was achieved by treatment with 1% 100X Triton following by blocking with 4% bovine serum albumin (BSA). Primary antibody for  $\gamma$ H2AX was incubated with coverslips overnight in 4°C. After incubation with secondary antibody conjugated to Alexaflour 488, coverslips were mounted to microscope

slides with mounting medium which contained nuclear DAPI stain and sealed before imaging. Fluorescence intensity was measured via ImageJ software.

### **3.4 Results**

#### **3.4.1 Split low dose radiation-induced carcinogenesis model.**

To investigate how PLK1 regulation of Mre11a can effect DDR *in vivo*, we first employed a split low dose radiation-induced carcinogenesis model. Studies demonstrated that split low dose radiation can induce mutational burden over time in the quiescent hematopoietic stem cell (HSC) population. As seen in **Fig 3.1A**, split low dose radiation is performed utilizing low doses of total body irradiation (TBI) exposure (2Gy) weekly for 4-5 weeks, inducing a total of 8-10Gy of TBI. For this study, animals were exposed for 4 weeks for a total of 8GY TBI. To monitor the impact of TBI on complete blood count (CBC) whole blood was collected 1 day prior to radiation exposure for every exposure using a HemaVet analyzer. As expected, following radiation induction on day 6, 12, 20, and 29, the total white blood cell count was drastically lower compared to the results from day 0 (**Fig 3.1B**) indicating that the treatment scheme was extinguishing most of the hematopoietic progenitor cells (HPC), but not all of the hematopoietic stem cells (HSC). In addition, a slow recovery of white blood cells was observed up to 139 days following irradiation. We see a similar trend in the neutrophil (**Fig 3.1C**) and lymphocyte (**Fig 3.1D**) populations as both of these cell types are white blood cells. The CBC results for red blood cell counts (**Fig 3.1E**) and platelets (**Fig 3.1F**) were generally unaffected by irradiation, which was expected. After the final treatment of 2Gy TBI, the mice were allowed to recover for 1 month, followed by blood

collection and flow cytometric analysis (**Fig 3.1G**). After gating for CD45.1+ and CD3+ cells, we observed single-stained CD8a and CD4 populations as well as CD8a/CD4 double positive and double negative populations. Immature T cells, characterized by a CD8a/CD4 double positive population, found in circulation is indicative of tumorigenesis. While these results were not significant for the induction of the double positive population, we observed an increasing trend in the radiation-induced mice to confirm the health of hematopoietic system (**Fig 3.1G**). As we continued to monitor both the health of the mice induced with IR as well as the double positive populations, we noticed a recovery of the immature T cells in circulation 2 months (**Fig 3.1H**) and 3 months (**Fig 3.1I**) post irradiation. At 5 months following IR, we observed a recurrence of the double positive population of CD8a/CD4 T cells in circulation and a decline in the health of some mice in our IR treatment groups (**Fig 3.1J**). Altogether, these results suggest validity in the rigor of the split low dose IR-induced carcinogenesis model for studying manipulations to the DDR pathway.

#### ***3.4.2 Carcinogenesis was not different between WT and Mre11a<sup>SSDD</sup> mice following split low dose radiation.***

Previous literature demonstrated the the latency period for thymic lymphoma disease development can vary between 100-500 days post-IR in the split low dose IR model [136-138]. In our study, we observed a phenotypic decline in 1 set of irradiated mice, one WT mouse and one Mre11a<sup>SSDD</sup> mouse, at 190 days post-IR. Upon sacrifice, we observed an enlarged spleen in the WT IR mouse which is a common indicator of disease development (data not shown) [139-141].

Following tissue collection, we performed flow cytometric analysis and observed drastic differences in the T cell populations of WT and Mre11a<sup>SSDD</sup> mice (**Fig 3.2B**). Generally, we observed an increase in CD8a+ cell populations in the WT mouse for both the peripheral blood and the thymus (**Fig 3.2C-D**). We expected that the thymus of control WT mice would contain primarily CD8a+/CD4+ double positive populations of T cells [95], in agreement, the irradiated Mre11a<sup>SSDD</sup> mouse also presented with the same double positive population of T cells. We expected that we would observe a similar shift to a CD8a single positive population as the WT mouse following IR, which is indicative of thymic lymphoma, but we were surprised to find that the thymus of the Mre11a<sup>SSDD</sup> mouse most closely resembled a normal control thymus (**Fig 3.2B-D**).

We next formalin fixation and paraffin embedding the harvested tissues for further investigation via IHC. Our results, revealed a difference in H&E staining for both the liver and spleen in each mouse (**Fig 3.2A**). While the spleen of the Mre11a<sup>SSDD</sup> mouse clearly exhibits distinct populations of white pulp/red pulp, the spleen of the WT mouse has become clearly homogenous where distinct splenic structures have become undetectable [142]. In addition, based on the H&E staining in the liver of both the Mre11a<sup>SSDD</sup> and WT mouse, we observed clear immune infiltration into the liver of the WT mouse whereas the Mre11a<sup>SSDD</sup> exhibited similar hepatocyte structure of a normal liver with plates of cells being separated by capillaries [143]. To solidify this evidence of immune infiltration of the liver, Ki67 staining (a known proliferation marker) indicated proliferation in the same liver regions in which immune infiltration was observed [144]. Similarly, we did not

observe a strong Ki67 signal in the IHC of Mre11a<sup>SSDD</sup> liver. Ki67 staining is visible within the spleen of the Mre11a<sup>SSDD</sup> mouse, however, almost the entire spleen of the WT mouse displayed prominent Ki67 staining suggesting a high level of proliferative cells. To confirm the nature of these proliferative cells, we stained tissue sections with CD3, CD8a, and CD4 [142, 145]. The most notable observation was the induction of CD3 and CD8a staining in the liver of the WT mouse where staining in the Mre11a<sup>SSDD</sup> mouse was completely absent. These findings together gave us confidence in the radiation-induced model of carcinogenesis and in the progression of this study.

To further investigate this phenotype, we sacrificed the other mice in both control groups, the WT-IR group and Mre11a<sup>SSDD</sup>-IR group. Upon collecting thymus, spleen, bone marrow, peripheral blood, and liver; we processed a portion of the thymus for single cell RNA sequencing (scRNA seq) which will be addressed in **Figure 3.3**. After cell preparation for flow cytometric analysis, our results did not demonstrate an observable difference in immature T cell populations between WT and Mre11a<sup>SSDD</sup> mice (**Figure 3.2E**). Compared to the control mice, the WT and Mre11a<sup>SSDD</sup> mice have similar trends in primarily double positive T cell populations in the thymus, and general CD8a single positive or double negative populations in the peripheral blood and bone marrow. Similarly, the H&E, Ki67, and CD3 staining of the spleen and thymus did not exhibit the same phenotype as the first pair of WT (**Fig 3.2F**) and Mre11a<sup>SSDD</sup> (**Fig 3.2G**) mice. These results together indicated no difference in the phenotype between WT and Mre11a<sup>SSDD</sup> mice after split low dose irradiation.

### ***3.4.3 scRNA sequencing preliminary analysis suggests a possible difference between Mre11a<sup>SSDD</sup> mice and WT after split low dose radiation.***

Utilizing the thymocytes collected from the split low dose irradiation mice in **Figure 3.2**, we processed the samples and subjected them to scRNA seq. Thymocytes were analyzed using batch analysis for specific lymphocyte/T cell markers such as CD45, CD3, CD8a, and CD4 (**Fig 3.2A**). Based on our initial findings we anticipate that there could be a difference in the RNA expression profiles in between treated WT and Mre11a<sup>SSDD</sup> mouse thymocytes, however, due to the small sample size, the differences is only suggested here (**Fig 3.2B-C**).

### ***3.4.4 Medium-high single dose treatment has no effect on the development of carcinogenesis in either Mre11a<sup>SSDD</sup> or WT mice.***

Although fractionated low dose radiation exposure is considered the gold standard in radiation-induced carcinogenesis, we wanted to investigate the effect that using a higher single dose of exposure would have on tumorigenesis. We treated WT and Mre11a<sup>SSDD</sup> mice with a single dose of 5Gy IR and phenotypically monitored disease development. After 11 months latency from IR exposure, mice in the WT and Mre11a<sup>SSDD</sup> groups both exhibited greying fur and were less active and we did not observe an obvious difference between groups. Upon sacrifice, we processed the tissues for flow cytometric analysis of T cell marker expression. Between control, WT-IR and Mre11a<sup>SSDD</sup>-IR groups, there was not a significant difference in CD8a+/CD4+ double positive populations in the peripheral blood, bone marrow, or spleen (**Fig 3.4A**). In addition, since the thymus is the location in which immature T cells are generated, the thymocytes in all 3 groups exhibited the

similar expected immature T cell double positive populations indicative of a lack of carcinogenesis in either IR treatment group. This experiment demonstrates the difference between single dose treatment at a higher exposure and multiple treatments at a lower exposure.

#### **3.4.5 *Mre11a*<sup>SSDD</sup> MEFs promote extension of $\gamma$ H<sub>2</sub>AX induction immediately following IR.**

To further investigate the radiation response *in vitro*, we harvested mouse embryonic fibroblasts (MEFs) and utilized DSB inducers to observe the DDR. MEFs were isolated, genotyped, and either induced with 1mM tamoxifen or vehicle for 48 hours prior to experimentation. We first tested the induction of  $\gamma$ H<sub>2</sub>AX following 3Gy IR in a time-dependent manner. Evidence demonstrates that induction of  $\gamma$ H<sub>2</sub>AX occurs as early as 15 minutes following IR, which is largely dissipated by 6 hours [146]. We observed the greatest  $\gamma$ H<sub>2</sub>AX induction at 30 minutes following IR with the signal starting to disappear around 4 hours (**Fig 3.5A**). However, quantification of the normalized band intensities between tamoxifen induced *Mre11a*<sup>SSDD</sup> MEFs and vehicle controls (WT) suggest a possible extension and longevity in this DDR signaling (**Fig 3.5A, bottom**). Utilizing a traditional cell viability assay, we tested the response of tamoxifen-induced *Mre11a*<sup>SSDD</sup> and WT MEFs to IR in a dose-dependent manner. We did not observe a difference in cell viability between MEF groups 72 hours post-IR (**Fig 3.5B**). We then tested 3 different DSB-inducers to determine whether the experimental conditions of the assay or the genotoxic challenge had the effect on cell viability as previously observed. After treating MEFs in a dose-dependent

manner with either Etoposide (**Fig 3.5C**), Camptothecin (**Fig 3.5D**), or Belomycin sulfate (**Fig 3.5E**); we again did not observe a difference in MEF cell viability following 72 hours of treatment (**Fig 3.5C-E** are n=1). Finally, we investigated whether the previously observed  $\gamma$ H<sub>2</sub>AX induction following IR occurred in a time-dependent manner, by immunofluorescence staining (**Fig 3.5F**). After quantifying the  $\gamma$ H<sub>2</sub>AX intensity per cell for each treatment group we observed an increasing trend of fluorescence intensity in tamoxifen-induced Mre11a<sup>SSDD</sup> MEFs compared to WT (**Fig 3.5G**). In addition, the calculated fluorescence intensity 4 hours post-IR for tamoxifen-induced Mre11a<sup>SSDD</sup> was significantly increased compared to WT (**Fig 3.5H**). Taken together, these results suggest possibly significant differences in response to IR immediately following DSB DNA damage and a lack of phenotype in a longer-term assay such as the traditional cell viability assay.

#### ***3.4.6 Lethal dose of IR induced survival does not differ between WT and Mre11a<sup>SSDD</sup> mice.***

To determine the effect of Mre11a<sup>SSDD</sup> on survival, we measured the length of survival following a lethal dose of IR of 8Gy (**Fig 3.6**). Due to hematopoietic failure, at 8Gy we would expect the survival of mice to be approximately between 7-14 days post-IR [147]. Indeed, we observed IR-induced death in both groups of mice primarily between 7-14 days post-IR, however, we did not observe a difference between WT and Mre11a<sup>SSDD</sup> mice indicating that Mre11a<sup>SSDD</sup> does not influence overall survival.

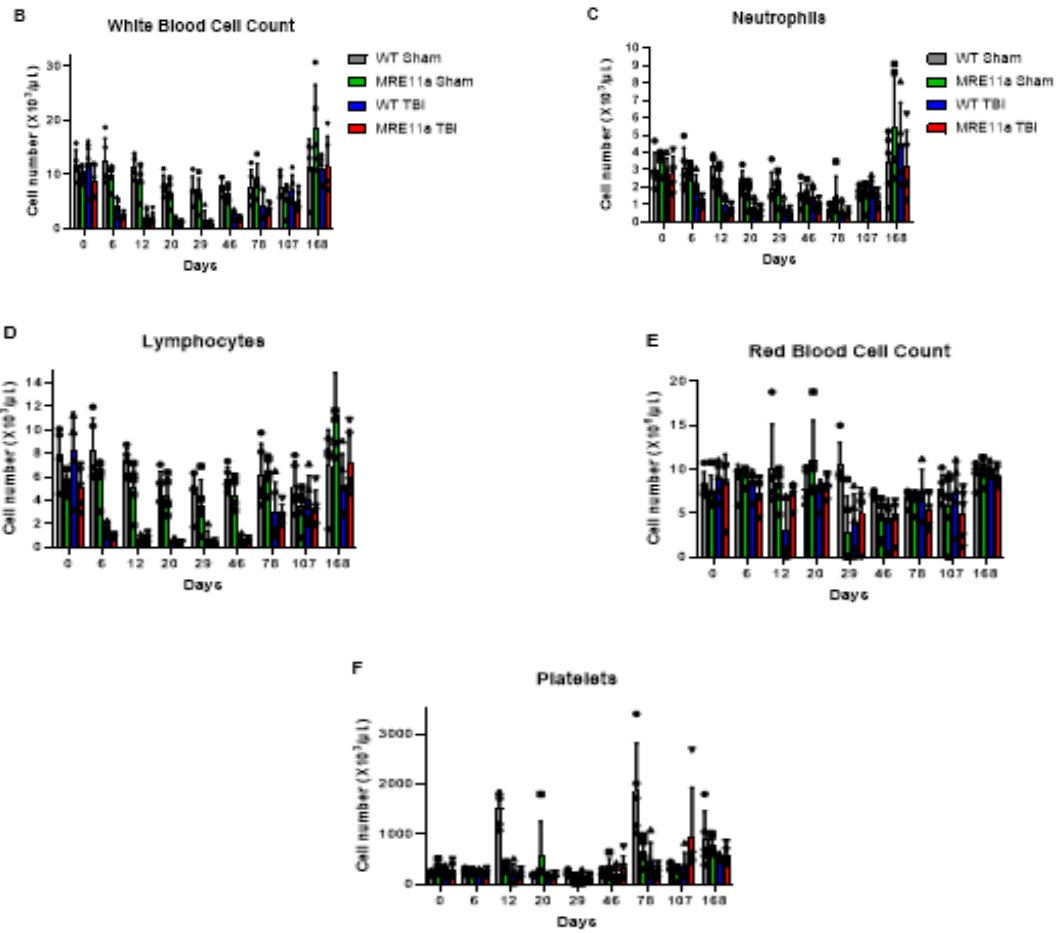
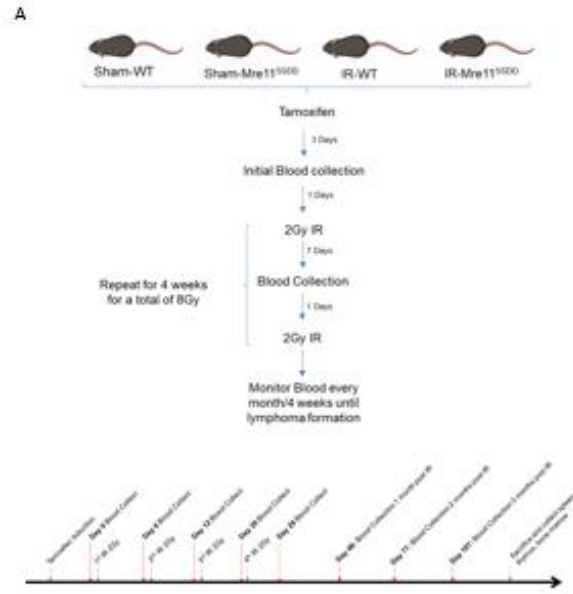
### 3.5 Discussion

DNA repair and the DNA damage response mechanisms have been studied for decades, however, novel regulators and non-canonical functions in regulatory proteins continue to be discovered. Generally, DNA must maintain a high rate of fidelity and stability for cellular function and maintenance which highlights the importance of the evolutionarily conserved mechanisms of DNA repair. Within the differing types of DNA repair, numerous mechanisms and checkpoints are in place to maintain the repair fidelity and promote tight regulation of these processes. PLK1, having recent implications in the regulation of some aspects of DNA damage repair, was observed to play a critical role in the regulation of MRN complex protein Mre11a. Our lab observed two phosphorylation events on Mre11a during G2 DNA damage checkpoint recovery. Plk1 phosphorylated Mre11a at S649 allowing for subsequent phosphorylation by CK2 at S686. These results demonstrated the phosphorylation-induced drive to prematurely terminate checkpoint 2 and therefore, inhibiting DNA damage repair in response to radiation-induced carcinogenesis. Following these results, our lab generated a GEM double mutant knock-in model of Mre11a knocking-in phospho-mimic mutations at the S649 and S686 sites for PLK1 and CK2 phosphorylation respectively.

In this study, we employed a split low dose radiation-induced carcinogenesis model to determine the effects of the phospho-mimic double mutant may have in response to radiation *in vivo*. Utilizing the fractionated low dose radiation treatment scheme, we observed a loss of lymphocytes after each radiation exposure indicating the cell death of HPCs while the recovery of

lymphocytes 1-month post-IR is indicative of the presence of HSCs (**Fig 3.1A-G**). We continued to monitor the induction of immature T cells into circulation up to 5 months post-IR (**Fig 3.1H-J**) until we observed disease progression in the phenotypic characteristics of treatment mice 190 days post-IR. Flow cytometric analysis of the peripheral blood and thymocytes in a pair of treatment mice indicate an induction of immature T cells into circulation and a malfunction of thymus in its ability to produce immature T cells (**Fig 3.3B-D**). Similarly, we observed a possible disease phenotype between treatment groups in IHC tissue analysis where Mre11a<sup>SSDD</sup> seemed to exhibit a prevention of disease induction (**Fig 3.2A**). Unfortunately, upon sacrifice of the other mice in both treatment groups, we did not observe the same phenotype in the peripheral blood, thymocytes, or in IHC tissue staining where there is no significant difference between split low dose radiation-induce carcinogenesis of WT or Mre11a<sup>SSDD</sup> mice (**Fig 3.2E-G**). To further understand the difference in disease state between WT and Mre11a<sup>SSDD</sup>, we collected thymocytes for scRNA-seq analysis (**Fig 3.3**). In the preliminary UMAP results, we do not observe large differences in RNA expression profiles between distinct T cell populations of control, WT, or Mre11a<sup>SSDD</sup> mice (**Fig 3.3A-B**). It is possible that further analysis could reveal a difference in treatment groups as the UMAP plot in **Fig 3.3C** demonstrates a large separation of cells from an Mre11a<sup>SSDD</sup> IR-treated mouse, however, an increased sample size would be necessary to provide conclusive evidence. In addition to the split low dose IR model, we also tested a single dose of medium-high IR exposure to observe differences in carcinogenesis between the WT and Mre11a<sup>SSDD</sup> mice (**Fig 3.4**).

After an 11 month latency from single dose exposure to IR, we sacrificed all groups and determined T cell populations via flow cytometric analysis. In alignment with the results of the split low dose IR-induced mice, we did not observe a significant difference in CD4/CD8a T cell populations. To investigate the effects of DSB induction on Mre11a<sup>SSDD</sup> double mutant *in vitro*, we harvested and utilized MEFs from the Mre11a<sup>SSDD</sup> mice (**Fig 3.5**). We first tested the effects of IR exposure on tamoxifen or vehicle induced Mre11a<sup>SSDD</sup> MEFs and observed slight differences in  $\gamma$ H<sub>2</sub>AX induction via immunoblotting in a time-dependent manner indicating a slightly delayed resolution of DNA damage in the Mre11a<sup>SSDD</sup> MEFs (**Fig 3.5A**). We tested this induction in a time-dependent manner utilizing immunofluorescence and observed a similar result to our immunoblotting data (**Fig 3.5F-H**). In addition, we subjected induced MEFs to various DSB inducers with no significant differences in cell viability (**Fig 3.5B-E**). Finally, we did not observe a difference in survival between WT and Mre11a<sup>SSDD</sup> following lethal exposure of IR (**Fig 3.6**). Together, the results of this study indicate a lack of difference in radiation-induced carcinogenesis of Mre11a<sup>SSDD</sup> mice and MEFs compared to WT.



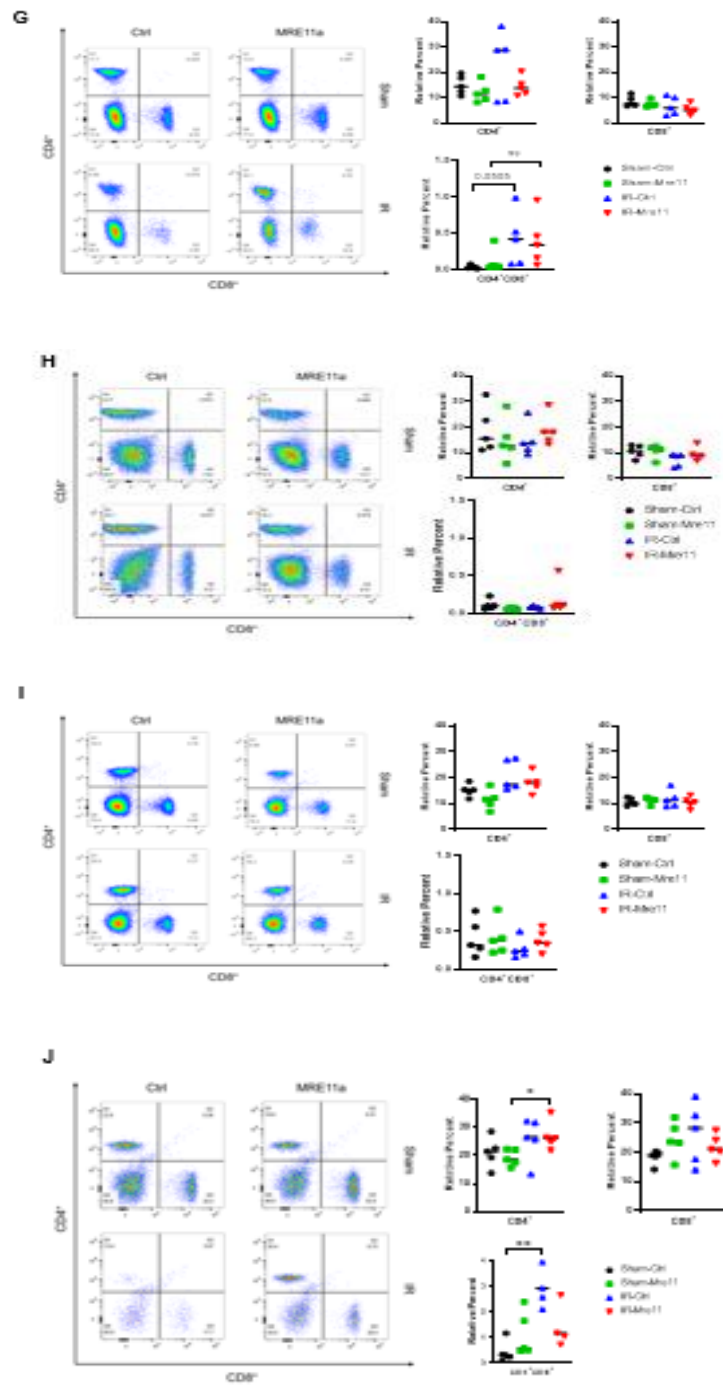


**Figure 3.1 Experimental design and thymic lymphoma monitoring of split low dose irradiation mice following treatment.**

Schematic representation of split low dose irradiation treatment regimen for induction of carcinogenesis **(A)**. CBC from whole blood Hemavet analysis of total white blood cells **(B)**, neutrophils **(C)**, lymphocytes **(D)**, red blood cell count **(E)**, and platelet **(F)** monitoring during irradiation treatment. Flow cytometric analysis of T cell markers for CD8a and/or CD4 positive population percentages at 1 month **(G)**, 2 months **(H)**, 3 months **(I)**, and 5 months **(J)** post-irradiation to monitor carcinogenesis induction. \*= $p \leq 0.05$ ; \*\*= $p \leq 0.01$ ; \*\*\*= $p \leq 0.001$ .

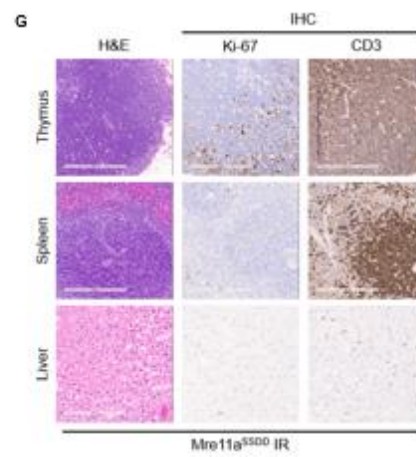
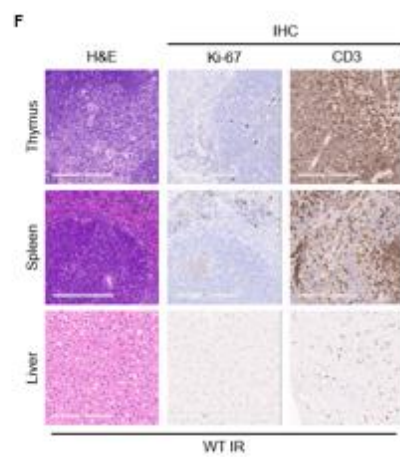
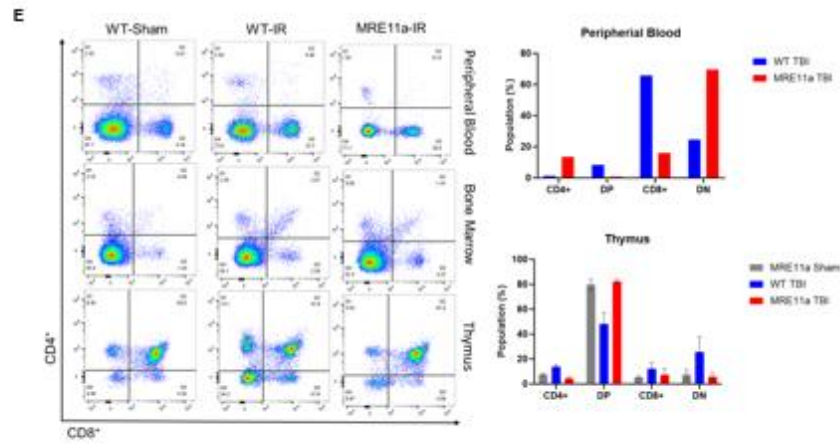
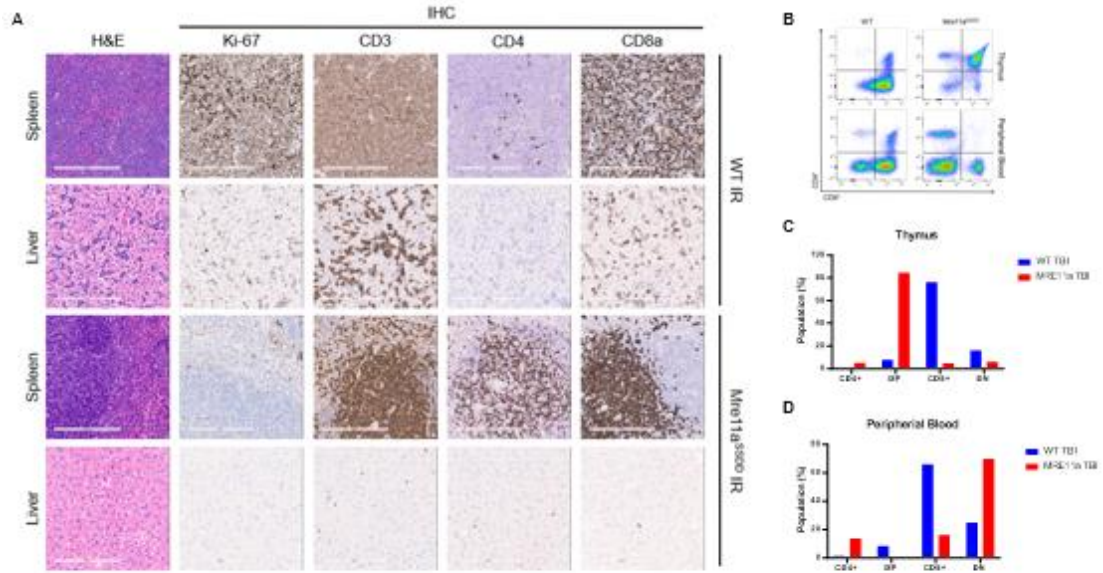


**Figure 3.2 IHC images and flow cytometric analysis of split low dose irradiation mice at harvest.**

H&E and IHC staining of liver and spleen tissue samples taken immediately after sacrifice 6 months post irradiation exposure **(A)**. Flow cytometric analysis of cells from tissues harvested 7 months post irradiation exposure **(B)**. Quantification of dot plots were taken as percentages of cell populations from parent CD3+/CD45.1+ cells. Representative H&E and IHC staining of thymus, liver and spleen tissue samples taken immediately after sacrifice 7 months post irradiation exposure for WT irradiated mice **(C)** and Mre11aSSDD irradiated mice **(D)**.

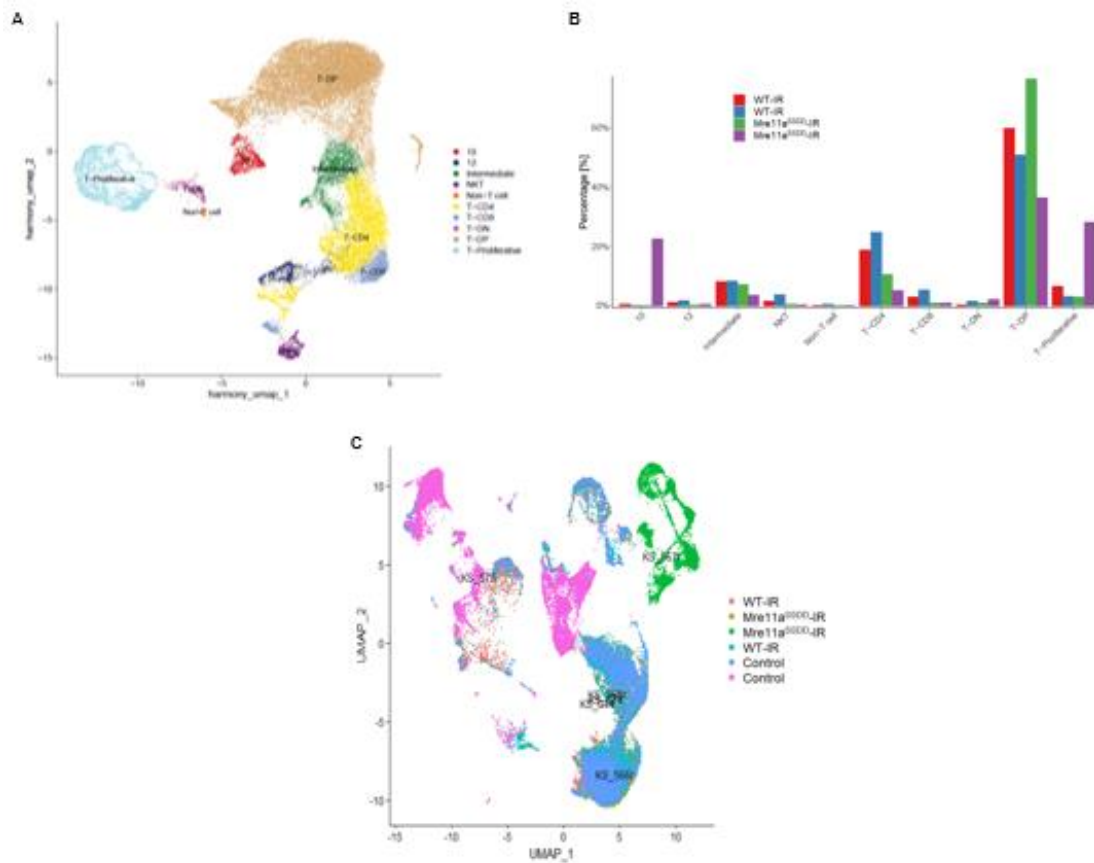


**Figure 3.3 scRNA-seq analysis suggests a possible RNA expression difference between both IR treated experimental groups.**

2D Harmony UMAP plot of thymocyte scRNA-seq data with 10 clusters **(A)**. Bar graph of prominent clusters organized by percentage per sample **(B)**. 2D UMAP plot separated by sample **(C)**. All plots were generated by the University of Kentucky's bioinformatics core.

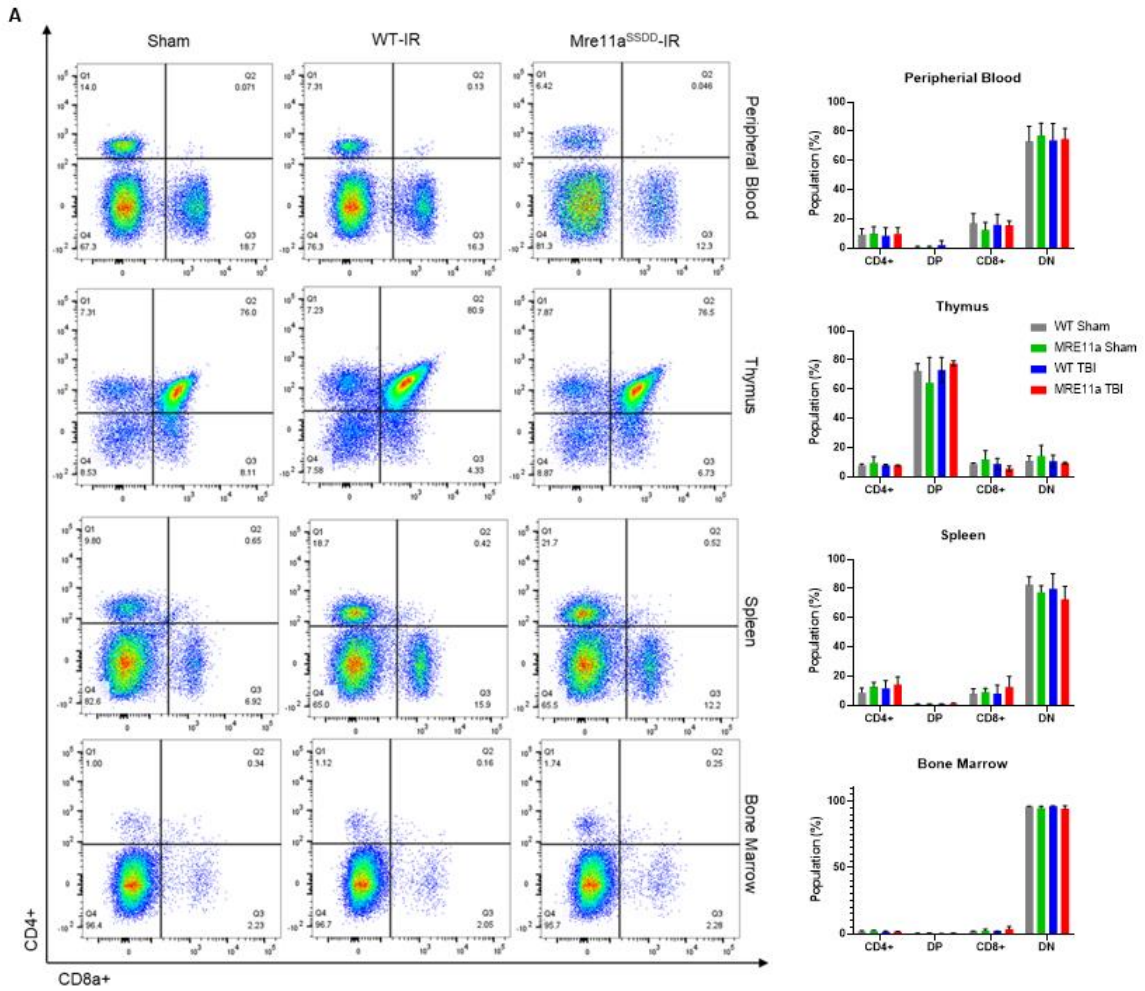


**Figure 3.4 Single dose radiation at 5Gy does not exhibit a radiation-induced carcinogenesis phenotype.**

Flow cytometric dot plot analysis of cells obtained from tissue samples that were purified immediately after sacrifice (**A**). Quantification of dot plots were taken as percentages of cell populations from parent CD3+/CD45.1+ cells.

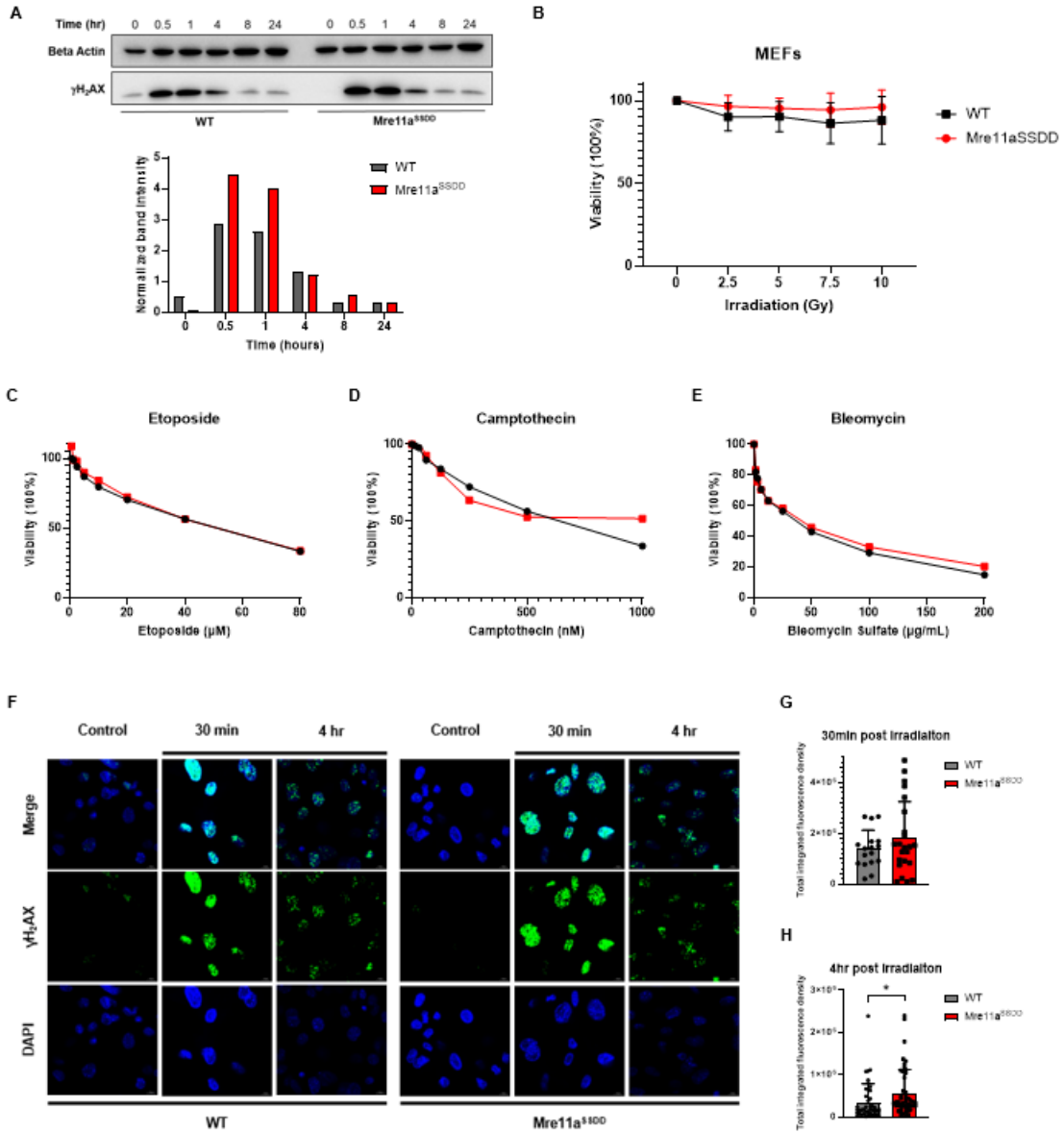


**Figure 3.5** Mre11a<sup>SSDD</sup> MEF DDR response to double strand break damage.

Immunoblotting (top) and quantification (bottom) of WT and Mre11a<sup>SSDD</sup> MEFs exposed to 3Gy radiation followed by collection at the indicated timepoints (**A**). Cell viability assay 72 hours following increasing doses of radiation (**B**). Data is scaled into percentage and normalized to untreated groups, then shown as mean  $\pm$ SD (n=3). Cell viability assays of MEFs exposure to differing doses of DNA double

strand break damage inducers etoposide **(C)**, camptothecin **(D)**, and bleomycin sulfate **(E)**. Data is scaled into percentage and normalized to untreated groups (n=1 for all 3 plots). Representative immunofluorescence images of WT and Mre11a<sup>SSDD</sup> MEFs following exposure to 3Gy radiation **(F)**. Total integrated fluorescence densities were calculated for 30 minutes post exposure **(G)** and 4 hours post exposure **(H)** using ImageJ software. Three fields were captured per treatment group with between 9-20 cells per field. CTCF was calculated using the following formula: CTCF = Integrated density – (area of selected cell \* mean fluorescence of background readings) to normalize the size and intensity of each cell and quantified where \*=p ≤ 0.05; \*\*=p ≤ 0.01; \*\*\*=p ≤ 0.001.

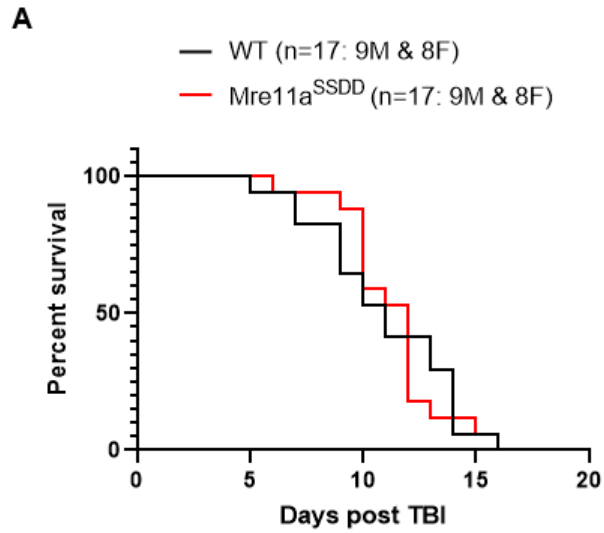


**Figure 3.6 Survival curve analysis of Mre11a<sup>SSDD</sup> mice.**

Kaplan-Meier survival curves of age-matched (6-8 weeks old) littermates of WT and Mre11a<sup>SSDD</sup> mice exposed to 8Gy single dose of TBI.

## CHAPTER 4. Conclusion and future directions

### 4.1 Conclusion

The results presented in chapter 2 of this dissertation demonstrate the critical need for continued research in drug-resistant CRPC. In many cancers, developed therapies successfully inhibit cancer progression, however, it is a common characteristic in cancers to overcome these challenges in treatment and in the case of this study, develop drug-resistance. Androgen receptor inhibitors in prostate cancer treatment aim to prevent the primary signaling mechanism driving PCa progression, however, this treatment over time leads to the development of drug-resistance and therefore, limited to no therapeutic options for advanced PCa patients. Recent evidence has suggested that CRPC relies on oxidative phosphorylation for glucose metabolism rather than increased lactate production observed in other cancers, demonstrating a possible vulnerability for treatment exploitation. This strategy is not uncommon in investigating new cancer treatments as energy metabolism in cancer typically functions differently than in normal cells, proving to be an attractive therapeutic target. We hypothesized that drug-resistant CRPC may be more vulnerable to enzalutamide treatment if treated in conjunction with metformin to inhibit OX PHOS.

As demonstrated previously, while combination treatment in drug-resistant CRPC cells exhibited a synergistic phenotype, the differences in mitochondrial function differed from the expected results and were not significant for mitochondrial modulation (**Fig 2.1-2.2**). Cells in these experiments were treated for 12- or 24-hour time periods before collection and analysis. To maintain the

proton gradient for ATP production, the MMP will continually shift and the mitochondria will adapt to challenge. Following 12- or 24- hours from treatment, the mitochondria has likely already overcome the challenges of treatment in the changes to the MMP and therefore, were not captured in this study. In a similar vein, observations of the changes in OCR following treatment were performed 12- to 24- hours following treatment. One possible explanation for a lack of difference in the combination treatment of drug-resistant CRPC lines, is that observable changes to the OCR and MMP may occur within the first few hours following treatment [148]. Another possible explanation for the unobserved differences in the mitochondrial function assays is the off-target effects of metformin. Not only does metformin inhibit complex I of the electron transport chain, but it has also been reported that metformin can inhibit complexes III and IV [149] as well as possibly inhibiting ATP synthase for overall modulation of OX PHOS [150]. Finally, consideration of the mechanisms in which our models have gained drug-resistance would possibly shed light on the inconsistencies observed in the *in vitro* results. There are many mechanisms in which cancer gains drug-resistance, both intrinsic and extrinsic and it would be important for future studies to identify these differences and consider them for future assays. As previously stated, 22Rv1 cells have an intrinsic resistance to enzalutamide by AR lacking the LBD for enzalutamide docking [97]. In the case of C4-2R and MR49F, these cells may have gained resistance in other mechanisms such as apoptosis pathway blocking [151], changes in drug metabolism [152], or alterations of epigenetic regulation

[153]. In this way, results from this study may differ from the expected outcomes due to these various factors in *in vitro* testing.

Similarly, we did not observe significant effects of combination treatment in either *in vivo* model tested demonstrating the extreme difficulty in the investigation for novel treatment strategies in drug-resistant cancers (**Fig 2.3-2.4**). An important point to consider is the pharmacokinetics of metformin. Specifically, drugs that enter organelles typically sequester and accumulate in the organelles of these cells, however, it has been demonstrated that metformin does not accumulate in the mitochondria as expected [154]. The discussion as to whether metformin's metabolic activity depends on its diffusion inside of cells is supported by some but not all studies investigating metformin [44]. In addition to accumulation differences within cells, metformin also targets various pathways such as the ETC, AMPK, and lipid metabolism [155]. It is well documented that metformin, in addition to inhibiting complex I of the ETC, activates AMPK for the inhibition of glucose production in primary hepatocytes [156]. Metformin has also been demonstrated to reduce hepatic steatosis in rodent liver thereby improving lipid metabolism *in vivo* [157] as well as in clinical trial [158]. The differences in accumulation as well as the off-target effects of metformin *in vivo* may be a possible explanation for the lack of significance *in vivo* for these studies. As stated previously, metformin is originally prescribed to patients with type 2 diabetes whose bodies cannot regulate excess glucose intake from diet. Similarly, mouse diet and individual resistance to insulin needs to be taken into consideration with the results of these *in vivo* studies.

Finally, changes to the techniques in which tumors were inoculated and drugs were administered may aid in bolstering an observable result between different treatment groups. While we were through in the inoculation of the PDX tumor subcutaneously, it may be more beneficial to homogenize the tumor from the host mouse first and subcutaneously inject tumor pieces with Matrigel rather than inoculating whole pieces of tumor. This would remove any concerns of the heterogeneity of the tumor cells within each mouse and improve the rigor of the study. Finally, we utilized oral administration of our treatments, however, to eliminate the factor of whether or not each mouse ingested the correct dose each time, utilizing an I.P. injection may be more accurate and reproducible in the future. Taken together with the phenotypic results in **Fig 2.1**, we expected a significant decrease in the RNA expression for cancer promoting signaling pathways such as Ras, mTOR and MAPK signaling, however, further validation of these findings is necessary (**Fig 2.5**).

The importance of functional and high-fidelity DNA repair mechanisms has been well documented for decades, however, the implications of non-DNA damage repair proteins in the regulation of repair mechanism are still under investigation. The mechanism in which the mitotic kinase, PLK1, orchestrates entry into mitosis is well documented but, its implications in regulation of other cellular mechanisms such as epigenetics, metabolism, and DNA damage repair are currently being investigated. Our lab has recently demonstrated the regulation of DNA repair protein Mre11a via phosphorylation in the G2 DNA damage checkpoint recovery to inhibit DNA damage repair in response to radiation-

induced carcinogenesis. Phosphorylation of Mre11a at S649 and S686 by PLK1 and CK2 respectively maintains the binding affinity of Mre11a to its partners, however, the induction of premature termination of the G2 checkpoint occurs.

In chapter 3 of this dissertation, we explored the relationship between IR induction and tumorigenesis in a thymic lymphoma model and how the double mutant knock-in phosphor-mimic of Mre11a responds to this damage compared to WT. Overall, we did observe smaller trends in the *in vivo* radiation-induced carcinogenesis models, however, significance between treatment groups was not observed and therefore, further testing is required to draw any conclusions (**Fig 3.1-3.4, 3.6**). One possible explanation for the lack of significance could be the small sample sizes used in the experiments. For IR treatment experiments, it is critical for the mice in the experiments to be littermates and age matched. In an experiment done by Dr. Shen's lab, all mice used in the experiments were age-matched and littermates when possible to avoid genetic variability [159]. Furthermore, while there is strong evidence that the Mre11a<sup>SSDD</sup> mutant has an impact on DDR capabilities *in vitro* [89], there are more complex compounding factors that may be at play *in vivo* to prevent a striking phenotype. In a mouse model without cancer, modulating the genotype to induce a double mutation on 1 protein may not have been enough to differentiate a phenotype between a normal mouse and an Mre11a<sup>SSDD</sup> mouse. In addition to increasing the sample size in each experiment, testing the induction of the tamoxifen using PCR would further confirm the model and experiment rigor.

Finally, it is important to speculate on the lack of thymic lymphoma development in all mice exposed to IR as this is the model we are utilizing to observe the modulation of DDR. There are a few factors to consider, the first being the machine that is exposing IR. Previously, our lab has utilized IR to induce DNA damage, however, in this study, we utilized a different method of IR exposure in x-ray irradiation [160]. Additionally, we utilized a similar experimental design as Dr. Shen's group in the induction of thymic lymphoma, however, the route of exposure was again different in that they utilized  $\gamma$ -rays for exposure [161]. The mice in the split-low dose experimental group were only exposed to a total of 8Gy TBI, whereas in Dr. Shen's experiments, the mice were exposed to at least 10Gy up to 12Gy of TBI [159]. This may also account for the lack of phenotype as the dosage for each experiment differed. In this manner, the exposure may not have been as uniform as originally hoped in addition to the differences in exposures and therefore, development of thymic lymphoma in all exposed groups may be different.

The only observable significant difference between WT and Mre11a<sup>SSDD</sup> was in the MEF IF  $\gamma$ H<sub>2</sub>AX induction following IR exposure where Mre11a<sup>SSDD</sup> MEFs exhibited prolonged/delayed DNA damage repair indicated by the extended signal of the  $\gamma$ H<sub>2</sub>AX foci (**Fig 3.5F**). While the results here have potential to have a significant phenotype, utilizing similar time points to determine the status of DNA repair in other manners such as a COMET assay, ligation assay, or a yeast two hybrid would bring validity to these results.

## 4.2 Future Directions

The results of this dissertation warrant future investigation including the following:

1. What other methods could be employed to test mitochondrial function after combination treatment *in vitro*?

In addition to the mito stress test, the glycolytic stress test and the glycolytic rate assay are two other seahorse assays utilized in measurement of mitochondrial function. The glycolytic rate assay specifically measures glycolysis and can capture passive and rapid responses to metabolic switches [162]. In this way, the glycolytic rate assay has an advantage over the traditional end-point lactate assay. Another method in measuring glycolysis is the glycolysis stress test. Specifically, this assay measures glycolytic function in key parameters of glycolytic efflux such as glycolysis, glycolytic capacity, glycolytic reserve, and nonglycolytic acidification [162].

2. Could the half-life of metformin be a contributing factor in the failure of the treatment regimen for *in vivo* dosing?

While metformin is an attractive candidate for cancer treatment, it only has a half-life of 12 hours *in vivo* [163]. In our study, mice were treated once a day for 5 days followed by 2 days off. In this manner, we may not have reached the maximum therapeutic efficacy during treatment. Additional studies where the treatment regimen included dosing twice a day, every day could be a more effective treatment strategy.

3. We observed an upregulation of RNA expression related to cell cycle in both ENZ-r cells. Could this finding suggest a possible different vulnerability that could be exploited as a novel therapeutic strategy?

Another facet of research interest in our lab is the regulation of cancer cell signaling pathways via PLK1 phosphorylation. As mentioned in chapter 3 of this dissertation, PLK1 is a critical mitotic regulator in the progression of cell cycle and is often upregulated in many cancer types [164]. Since we observed an increase in RNA expression profiles in cell cycle, it could be possible that metformin would have better efficacy in the attenuation of drug-resistant CRPC when treated in combination with PLK1 inhibitors.

4. Regarding Mre11a<sup>SSDD</sup> mutant and its response to radiation-induced carcinogenesis, further investigation utilizing a larger sample size may yield more conclusive results.

For all mouse experiments (except the survival curve) we utilized 5 mice per treatment group. With high variation between mice in *in vivo* studies, more individuals per group would increase the scientific rigor and reproducibility in this study. This can be seen in the vast difference of responses to split low dose radiation where the first pair of mice exhibited a possible difference between disease phenotypes, however, the result was not recapitulated in the rest of the mice in the study.

5. Utilizing the cultured MEFs in additional experiments may be another direction to further determine the exact response that MEFs may have to DSB.

While *in vivo* models have the best chance in representing how radiation-induced carcinogenesis can progress, further *in vitro* analysis of DNA damage response, repair efficacy, DNA damage variation, etc. utilizing the MEF models would enhance our understanding of the Mre11a<sup>SSDD</sup> mutant in the presence of radiation.

6. The Mre11a<sup>SSDD</sup> mutant, in our study, did not exhibit a significant effect on disease progression, however, this could be due to the model in which we investigated this response.

While our lab has previously observed a difference in repair efficacy between Mre11a double mutant, these results were investigated in U2OS bone cancer cells. It could be possible that we did not observe significant differences in disease progression because there are additional adaptations in cancer development that U2OS cells may possess, despite U2OS cells being proficient in DNA repair [165].

## APPENDIX

ADT	Androgen deprivation therapy
AR	Androgen receptor
ARE	Androgen response elements
ATM	Ataxia-telangiectasia mutated
BPH	Benign prostatic hyperplasia
Chk2	Checkpoint kinase 2
CK2	Casein kinase 2
CRPC	Castration resistant prostate cancer
CSPC	Castration sensitive prostate cancer
CSPC	Castration sensitive prostate cancer
CTCF	Corrected total cell fluorescence
DHT	Dihydrotestosterone
DSB	Double strand breaks
ENZ-r	Enzalutamide resistant
ETC	Electron transport chain
FCCP	Carbonyl cyanide-p-trifluoromethoxyphenylhydrazone
GEM	Genetically engineered mouse
HR	Homologous recombination
HSA	Highest single agent
HSP	Heat shock protein
IR	Ionizing radiation

LBD	Ligand binding domain
MDC1	Mediator of DNA damage checkpoint 1
MEF1	Mouse embryonic fibroblasts
MMP	Mitochondrial membrane potential
Mre11a	meiotic recombination 11 homolog 1
MRN	MRE11-RAD50-NBS1
OCR	Oxygen consumption rate
PCa	Prostate cancer
PLK1	Polo-like kinase 1
PSA	Prostate specific antigen
RPA	Replication protein A
scRNA-Seq	Single cell RNA sequencing
SSB	Single strand breaks
UMAP	Uniform manifold approximation and projection
$\gamma$ H <sub>2</sub> AX	Histone variant H2AX

## REFERENCES

1. Siegel, R.L., et al., *Cancer statistics, 2023*. CA Cancer J Clin, 2023. **73**(1): p. 17-48.
2. Rawla, P., *Epidemiology of Prostate Cancer*. World J Oncol, 2019. **10**(2): p. 63-89.
3. Sharifi, N., J.L. Gulley, and W.L. Dahut, *Androgen deprivation therapy for prostate cancer*. JAMA, 2005. **294**(2): p. 238-44.
4. Bambury, R.M. and H.I. Scher, *Enzalutamide: Development from bench to bedside*. Urol Oncol, 2015. **33**(6): p. 280-8.
5. Cutruzzola, F., et al., *Glucose Metabolism in the Progression of Prostate Cancer*. Front Physiol, 2017. **8**: p. 97.
6. Chen, C.L., C.Y. Lin, and H.J. Kung, *Targeting Mitochondrial OXPHOS and Their Regulatory Signals in Prostate Cancers*. Int J Mol Sci, 2021. **22**(24).
7. Mayer, M.J., L.H. Klotz, and V. Venkateswaran, *Metformin and prostate cancer stem cells: a novel therapeutic target*. Prostate Cancer Prostatic Dis, 2015. **18**(4): p. 303-9.
8. White, M.C., et al., *Age and cancer risk: a potentially modifiable relationship*. Am J Prev Med, 2014. **46**(3 Suppl 1): p. S7-15.
9. Bechis, S.K., P.R. Carroll, and M.R. Cooperberg, *Impact of age at diagnosis on prostate cancer treatment and survival*. J Clin Oncol, 2011. **29**(2): p. 235-41.

10. Brandao, A., P. Paulo, and M.R. Teixeira, *Hereditary Predisposition to Prostate Cancer: From Genetics to Clinical Implications*. Int J Mol Sci, 2020. **21**(14).
11. Knudsen, B.S. and V. Vasioukhin, *Mechanisms of prostate cancer initiation and progression*. Adv Cancer Res, 2010. **109**: p. 1-50.
12. Dunn, M.W. and M.W. Kazer, *Prostate cancer overview*. Semin Oncol Nurs, 2011. **27**(4): p. 241-50.
13. Ziada, A., M. Rosenblum, and E.D. Crawford, *Benign prostatic hyperplasia: an overview*. Urology, 1999. **53**(3 Suppl 3a): p. 1-6.
14. Sturge, J., M.P. Caley, and J. Waxman, *Bone metastasis in prostate cancer: emerging therapeutic strategies*. Nat Rev Clin Oncol, 2011. **8**(6): p. 357-68.
15. Berish, R.B., et al., *Translational models of prostate cancer bone metastasis*. Nat Rev Urol, 2018. **15**(7): p. 403-421.
16. Pound, C.R., et al., *Natural history of progression after PSA elevation following radical prostatectomy*. JAMA, 1999. **281**(17): p. 1591-7.
17. Gomella, L.G., J. Johannes, and E.J. Trabulsi, *Current prostate cancer treatments: effect on quality of life*. Urology, 2009. **73**(5 Suppl): p. S28-35.
18. Shoag, J.E., et al., *Reconsidering the Trade-offs of Prostate Cancer Screening*. N Engl J Med, 2020. **382**(25): p. 2465-2468.
19. Chandrasekar, T., et al., *Mechanisms of resistance in castration-resistant prostate cancer (CRPC)*. Transl Androl Urol, 2015. **4**(3): p. 365-80.

20. Cornford, P., et al., *EAU-ESTRO-SIOG Guidelines on Prostate Cancer. Part II: Treatment of Relapsing, Metastatic, and Castration-Resistant Prostate Cancer*. Eur Urol, 2017. **71**(4): p. 630-642.
21. He, L., et al., *Metastatic castration-resistant prostate cancer: Academic insights and perspectives through bibliometric analysis*. Medicine (Baltimore), 2020. **99**(15): p. e19760.
22. Tang, F., et al., *Chromatin profiles classify castration-resistant prostate cancers suggesting therapeutic targets*. Science, 2022. **376**(6596): p. eabe1505.
23. Hannu, K., M. Johanna, and S. Ulf-Hakan, *KLK-targeted Therapies for Prostate Cancer*. EJIFCC, 2014. **25**(2): p. 207-18.
24. Beltran, H., et al., *Molecular characterization of neuroendocrine prostate cancer and identification of new drug targets*. Cancer Discov, 2011. **1**(6): p. 487-95.
25. Yamada, Y. and H. Beltran, *Clinical and Biological Features of Neuroendocrine Prostate Cancer*. Curr Oncol Rep, 2021. **23**(2): p. 15.
26. Ojo, D., et al., *Prostate Cancer Stem-like Cells Contribute to the Development of Castration-Resistant Prostate Cancer*. Cancers (Basel), 2015. **7**(4): p. 2290-308.
27. Yokoyama, N.N., et al., *Wnt signaling in castration-resistant prostate cancer: implications for therapy*. Am J Clin Exp Urol, 2014. **2**(1): p. 27-44.

28. Hoffman-Censits, J. and W.K. Kelly, *Enzalutamide: a novel antiandrogen for patients with castrate-resistant prostate cancer*. Clin Cancer Res, 2013. **19**(6): p. 1335-9.
29. Wang, Y., et al., *Mechanisms of enzalutamide resistance in castration-resistant prostate cancer and therapeutic strategies to overcome it*. Br J Pharmacol, 2021. **178**(2): p. 239-261.
30. Litwin, M.S. and H.J. Tan, *The Diagnosis and Treatment of Prostate Cancer: A Review*. JAMA, 2017. **317**(24): p. 2532-2542.
31. Lonergan, P.E. and D.J. Tindall, *Androgen receptor signaling in prostate cancer development and progression*. J Carcinog, 2011. **10**: p. 20.
32. Handelsman, D.J., *Androgen Physiology, Pharmacology, Use and Misuse*, in *Endotext*, K.R. Feingold, et al., Editors. 2000: South Dartmouth (MA).
33. Smith, D.F. and D.O. Toft, *Minireview: the intersection of steroid receptors with molecular chaperones: observations and questions*. Mol Endocrinol, 2008. **22**(10): p. 2229-40.
34. van Royen, M.E., et al., *Compartmentalization of androgen receptor protein-protein interactions in living cells*. J Cell Biol, 2007. **177**(1): p. 63-72.
35. Bennett, N.C., et al., *Molecular cell biology of androgen receptor signalling*. Int J Biochem Cell Biol, 2010. **42**(6): p. 813-27.
36. Jin, H.J., J. Kim, and J. Yu, *Androgen receptor genomic regulation*. Transl Androl Urol, 2013. **2**(3): p. 157-177.

37. Lu, C. and J. Luo, *Decoding the androgen receptor splice variants*. *Transl Androl Urol*, 2013. **2**(3): p. 178-186.
38. Hornberg, E., et al., *Expression of androgen receptor splice variants in prostate cancer bone metastases is associated with castration-resistance and short survival*. *PLoS One*, 2011. **6**(4): p. e19059.
39. Hu, R., et al., *Ligand-independent androgen receptor variants derived from splicing of cryptic exons signify hormone-refractory prostate cancer*. *Cancer Res*, 2009. **69**(1): p. 16-22.
40. Sobhani, N., et al., *AR-V7 in Metastatic Prostate Cancer: A Strategy beyond Redemption*. *Int J Mol Sci*, 2021. **22**(11).
41. Liberti, M.V. and J.W. Locasale, *The Warburg Effect: How Does it Benefit Cancer Cells?* *Trends Biochem Sci*, 2016. **41**(3): p. 211-218.
42. Doherty, J.R. and J.L. Cleveland, *Targeting lactate metabolism for cancer therapeutics*. *J Clin Invest*, 2013. **123**(9): p. 3685-92.
43. Kozal, K., P. Jozwiak, and A. Krzeslak, *Contemporary Perspectives on the Warburg Effect Inhibition in Cancer Therapy*. *Cancer Control*, 2021. **28**: p. 10732748211041243.
44. Fontaine, E., *Metformin-Induced Mitochondrial Complex I Inhibition: Facts, Uncertainties, and Consequences*. *Front Endocrinol (Lausanne)*, 2018. **9**: p. 753.
45. Bailey, C.J. and R.C. Turner, *Metformin*. *N Engl J Med*, 1996. **334**(9): p. 574-9.

46. Foretz, M., B. Guigas, and B. Viollet, *Understanding the glucoregulatory mechanisms of metformin in type 2 diabetes mellitus*. Nat Rev Endocrinol, 2019. **15**(10): p. 569-589.
47. Viollet, B., et al., *Cellular and molecular mechanisms of metformin: an overview*. Clin Sci (Lond), 2012. **122**(6): p. 253-70.
48. LaMoia, T.E. and G.I. Shulman, *Cellular and Molecular Mechanisms of Metformin Action*. Endocr Rev, 2021. **42**(1): p. 77-96.
49. Noto, H., et al., *Cancer risk in diabetic patients treated with metformin: a systematic review and meta-analysis*. PLoS One, 2012. **7**(3): p. e33411.
50. Masarwa, R., et al., *Efficacy and Safety of Metformin for Obesity: A Systematic Review*. Pediatrics, 2021. **147**(3).
51. Whitburn, J., C.M. Edwards, and P. Sooriakumaran, *Metformin and Prostate Cancer: a New Role for an Old Drug*. Curr Urol Rep, 2017. **18**(6): p. 46.
52. Dowling, R.J., et al., *Metformin inhibits mammalian target of rapamycin-dependent translation initiation in breast cancer cells*. Cancer Res, 2007. **67**(22): p. 10804-12.
53. Rizos, C.V. and M.S. Elisaf, *Metformin and cancer*. Eur J Pharmacol, 2013. **705**(1-3): p. 96-108.
54. Sleire, L., et al., *Drug repurposing in cancer*. Pharmacol Res, 2017. **124**: p. 74-91.
55. Zhang, Z., et al., *Overcoming cancer therapeutic bottleneck by drug repurposing*. Signal Transduct Target Ther, 2020. **5**(1): p. 113.

56. Bayat Mokhtari, R., et al., *Combination therapy in combating cancer*. Oncotarget, 2017. **8**(23): p. 38022-38043.
57. Aravind, L., D.R. Walker, and E.V. Koonin, *Conserved domains in DNA repair proteins and evolution of repair systems*. Nucleic Acids Res, 1999. **27**(5): p. 1223-42.
58. Aguilera, A. and T. Garcia-Muse, *Causes of genome instability*. Annu Rev Genet, 2013. **47**: p. 1-32.
59. Casey, G., *The BRCA1 and BRCA2 breast cancer genes*. Curr Opin Oncol, 1997. **9**(1): p. 88-93.
60. Patel, K.J., et al., *Involvement of Brca2 in DNA repair*. Mol Cell, 1998. **1**(3): p. 347-57.
61. Sieber, O.M., K. Heinemann, and I.P. Tomlinson, *Genomic instability--the engine of tumorigenesis?* Nat Rev Cancer, 2003. **3**(9): p. 701-8.
62. Salmaninejad, A., et al., *Genomic Instability in Cancer: Molecular Mechanisms and Therapeutic Potentials*. Curr Pharm Des, 2021. **27**(28): p. 3161-3169.
63. Dasari, S. and P.B. Tchounwou, *Cisplatin in cancer therapy: molecular mechanisms of action*. Eur J Pharmacol, 2014. **740**: p. 364-78.
64. Ranasinghe, R., M.L. Mathai, and A. Zulli, *Cisplatin for cancer therapy and overcoming chemoresistance*. Heliyon, 2022. **8**(9): p. e10608.
65. Friedberg, E.C., *DNA damage and repair*. Nature, 2003. **421**(6921): p. 436-40.

66. Abbotts, R. and D.M. Wilson, 3rd, *Coordination of DNA single strand break repair*. Free Radic Biol Med, 2017. **107**: p. 228-244.
67. Kanaar, R., J.H. Hoeijmakers, and D.C. van Gent, *Molecular mechanisms of DNA double strand break repair*. Trends Cell Biol, 1998. **8**(12): p. 483-9.
68. San Filippo, J., P. Sung, and H. Klein, *Mechanism of eukaryotic homologous recombination*. Annu Rev Biochem, 2008. **77**: p. 229-57.
69. Burma, S., B.P. Chen, and D.J. Chen, *Role of non-homologous end joining (NHEJ) in maintaining genomic integrity*. DNA Repair (Amst), 2006. **5**(9-10): p. 1042-8.
70. Lamarche, B.J., N.I. Orazio, and M.D. Weitzman, *The MRN complex in double-strand break repair and telomere maintenance*. FEBS Lett, 2010. **584**(17): p. 3682-95.
71. Wang, Q., et al., *Rad17 recruits the MRE11-RAD50-NBS1 complex to regulate the cellular response to DNA double-strand breaks*. EMBO J, 2014. **33**(8): p. 862-77.
72. McCarthy-Leo, C., F. Darwiche, and M.A. Tainsky, *DNA Repair Mechanisms, Protein Interactions and Therapeutic Targeting of the MRN Complex*. Cancers (Basel), 2022. **14**(21).
73. Wu, L., et al., *MDC1 regulates intra-S-phase checkpoint by targeting NBS1 to DNA double-strand breaks*. Proc Natl Acad Sci U S A, 2008. **105**(32): p. 11200-5.

74. Mahaney, B.L., K. Meek, and S.P. Lees-Miller, *Repair of ionizing radiation-induced DNA double-strand breaks by non-homologous end-joining*. *Biochem J*, 2009. **417**(3): p. 639-50.
75. Shamanna, R.A., et al., *WRN regulates pathway choice between classical and alternative non-homologous end joining*. *Nat Commun*, 2016. **7**: p. 13785.
76. Grabarz, A., et al., *A role for BLM in double-strand break repair pathway choice: prevention of CtIP/Mre11-mediated alternative nonhomologous end-joining*. *Cell Rep*, 2013. **5**(1): p. 21-8.
77. Syed, A. and J.A. Tainer, *The MRE11-RAD50-NBS1 Complex Conducts the Orchestration of Damage Signaling and Outcomes to Stress in DNA Replication and Repair*. *Annu Rev Biochem*, 2018. **87**: p. 263-294.
78. Krejci, L., et al., *Homologous recombination and its regulation*. *Nucleic Acids Res*, 2012. **40**(13): p. 5795-818.
79. Lafrance-Vanasse, J., G.J. Williams, and J.A. Tainer, *Envisioning the dynamics and flexibility of Mre11-Rad50-Nbs1 complex to decipher its roles in DNA replication and repair*. *Prog Biophys Mol Biol*, 2015. **117**(2-3): p. 182-193.
80. Tomimatsu, N., et al., *Exo1 plays a major role in DNA end resection in humans and influences double-strand break repair and damage signaling decisions*. *DNA Repair (Amst)*, 2012. **11**(4): p. 441-8.

81. Ramani, P., et al., *High levels of polo-like kinase 1 and phosphorylated translationally controlled tumor protein indicate poor prognosis in neuroblastomas*. J Neurooncol, 2015. **125**(1): p. 103-11.
82. Tut, T.G., et al., *Upregulated Polo-Like Kinase 1 Expression Correlates with Inferior Survival Outcomes in Rectal Cancer*. PLoS One, 2015. **10**(6): p. e0129313.
83. Zhang, R., et al., *Misregulation of polo-like protein kinase 1, P53 and P21WAF1 in epithelial ovarian cancer suggests poor prognosis*. Oncol Rep, 2015. **33**(3): p. 1235-42.
84. Barr, F.A., H.H. Sillje, and E.A. Nigg, *Polo-like kinases and the orchestration of cell division*. Nat Rev Mol Cell Biol, 2004. **5**(6): p. 429-40.
85. McKenzie, L., et al., *p53-dependent repression of polo-like kinase-1 (PLK1)*. Cell Cycle, 2010. **9**(20): p. 4200-12.
86. Zhu, H., et al., *Identification of promoter elements responsible for transcriptional inhibition of polo-like kinase 1 and topoisomerase IIalpha genes by p21(WAF1/CIP1/SDI1)*. Cell Cycle, 2002. **1**(1): p. 59-66.
87. Lu, R., et al., *Post-Translational Modification of MRE11: Its Implication in DDR and Diseases*. Genes (Basel), 2021. **12**(8).
88. Simoneau, A., et al., *Cdk1-dependent regulation of the Mre11 complex couples DNA repair pathways to cell cycle progression*. Cell Cycle, 2014. **13**(7): p. 1078-90.
89. Li, Z., et al., *Plk1 Phosphorylation of Mre11 Antagonizes the DNA Damage Response*. Cancer Res, 2017. **77**(12): p. 3169-3180.

90. Ryan, J.L., *Ionizing radiation: the good, the bad, and the ugly*. J Invest Dermatol, 2012. **132**(3 Pt 2): p. 985-93.
91. Mavragani, I.V., et al., *Complex DNA Damage: A Route to Radiation-Induced Genomic Instability and Carcinogenesis*. Cancers (Basel), 2017. **9**(7).
92. Boniver, J., et al., *Cellular aspects of the pathogenesis of radiation--induced thymic lymphomas in C57 BL mice (review)*. In Vivo, 1990. **4**(1): p. 41-3.
93. Mothersill, C. and C. Seymour, *Low-dose radiation effects: experimental hematology and the changing paradigm*. Exp Hematol, 2003. **31**(6): p. 437-45.
94. Owen, D.L., L.E. Sjaastad, and M.A. Farrar, *Regulatory T Cell Development in the Thymus*. J Immunol, 2019. **203**(8): p. 2031-2041.
95. Introcaso, C.E., et al., *CD8+ epidermotropic cytotoxic T-cell lymphoma with peripheral blood and central nervous system involvement*. Arch Dermatol, 2008. **144**(8): p. 1027-9.
96. Ritch, C.R. and M.S. Cookson, *Advances in the management of castration resistant prostate cancer*. BMJ, 2016. **355**: p. i4405.
97. Antonarakis, E.S., et al., *AR-V7 and resistance to enzalutamide and abiraterone in prostate cancer*. N Engl J Med, 2014. **371**(11): p. 1028-38.
98. Efsthathiou, E., et al., *Molecular characterization of enzalutamide-treated bone metastatic castration-resistant prostate cancer*. Eur Urol, 2015. **67**(1): p. 53-60.

99. van Soest, R.J., et al., *Targeting the Androgen Receptor Confers In Vivo Cross-resistance Between Enzalutamide and Docetaxel, But Not Cabazitaxel, in Castration-resistant Prostate Cancer*. *Eur Urol*, 2015. **67**(6): p. 981-985.
100. Kasznicki, J., A. Sliwinska, and J. Drzewoski, *Metformin in cancer prevention and therapy*. *Ann Transl Med*, 2014. **2**(6): p. 57.
101. Zhao, Y., et al., *Combination of metformin and paclitaxel suppresses proliferation and induces apoptosis of human prostate cancer cells via oxidative stress and targeting the mitochondria-dependent pathway*. *Oncol Lett*, 2019. **17**(5): p. 4277-4284.
102. Ben Sahra, I., et al., *The antidiabetic drug metformin exerts an antitumoral effect in vitro and in vivo through a decrease of cyclin D1 level*. *Oncogene*, 2008. **27**(25): p. 3576-86.
103. Kong, Y., et al., *Inhibition of EZH2 Enhances the Antitumor Efficacy of Metformin in Prostate Cancer*. *Mol Cancer Ther*, 2020. **19**(12): p. 2490-2501.
104. Shao, C., et al., *Inhibition of polo-like kinase 1 (Plk1) enhances the antineoplastic activity of metformin in prostate cancer*. *J Biol Chem*, 2015. **290**(4): p. 2024-33.
105. Chen, L., N. Ahmad, and X. Liu, *Combining p53 stabilizers with metformin induces synergistic apoptosis through regulation of energy metabolism in castration-resistant prostate cancer*. *Cell Cycle*, 2016. **15**(6): p. 840-9.

106. Spratt, D.E., et al., *Metformin and prostate cancer: reduced development of castration-resistant disease and prostate cancer mortality*. Eur Urol, 2013. **63**(4): p. 709-16.
107. Murtola, T.J., et al., *Antidiabetic medication and prostate cancer risk: a population-based case-control study*. Am J Epidemiol, 2008. **168**(8): p. 925-31.
108. Rothermundt, C., et al., *Metformin in chemotherapy-naive castration-resistant prostate cancer: a multicenter phase 2 trial (SAKK 08/09)*. Eur Urol, 2014. **66**(3): p. 468-74.
109. Bai, Y., et al., *Inhibition of enhancer of zeste homolog 2 (EZH2) overcomes enzalutamide resistance in castration-resistant prostate cancer*. J Biol Chem, 2019. **294**(25): p. 9911-9923.
110. Horan, M.P., N. Pichaud, and J.W. Ballard, *Review: quantifying mitochondrial dysfunction in complex diseases of aging*. J Gerontol A Biol Sci Med Sci, 2012. **67**(10): p. 1022-35.
111. Ferrick, D.A., A. Neilson, and C. Beeson, *Advances in measuring cellular bioenergetics using extracellular flux*. Drug Discov Today, 2008. **13**(5-6): p. 268-74.
112. Sukumar, M., et al., *Mitochondrial Membrane Potential Identifies Cells with Enhanced Stemness for Cellular Therapy*. Cell Metab, 2016. **23**(1): p. 63-76.
113. Weber, M.J. and D. Gioeli, *Ras signaling in prostate cancer progression*. J Cell Biochem, 2004. **91**(1): p. 13-25.

114. Edlind, M.P. and A.C. Hsieh, *PI3K-AKT-mTOR signaling in prostate cancer progression and androgen deprivation therapy resistance*. Asian J Androl, 2014. **16**(3): p. 378-86.
115. Shorning, B.Y., et al., *The PI3K-AKT-mTOR Pathway and Prostate Cancer: At the Crossroads of AR, MAPK, and WNT Signaling*. Int J Mol Sci, 2020. **21**(12).
116. Rodriguez-Berriguete, G., et al., *MAP Kinases and Prostate Cancer*. J Signal Transduct, 2012. **2012**: p. 169170.
117. Seruga, B., A. Ocana, and I.F. Tannock, *Drug resistance in metastatic castration-resistant prostate cancer*. Nat Rev Clin Oncol, 2011. **8**(1): p. 12-23.
118. Amaral, T.M., et al., *Castration-resistant prostate cancer: mechanisms, targets, and treatment*. Prostate Cancer, 2012. **2012**: p. 327253.
119. Berenbaum, M.C., *What is synergy?* Pharmacol Rev, 1989. **41**(2): p. 93-141.
120. Mookerjee, S.A. and M.D. Brand, *Measurement and Analysis of Extracellular Acid Production to Determine Glycolytic Rate*. J Vis Exp, 2015(106): p. e53464.
121. Westermann, B., *Bioenergetic role of mitochondrial fusion and fission*. Biochim Biophys Acta, 2012. **1817**(10): p. 1833-8.
122. Sarwar, M., et al., *Targeted suppression of AR-V7 using PIP5K1alpha inhibitor overcomes enzalutamide resistance in prostate cancer cells*. Oncotarget, 2016. **7**(39): p. 63065-63081.

123. Kregel, S., et al., *Androgen receptor degraders overcome common resistance mechanisms developed during prostate cancer treatment*. Neoplasia, 2020. **22**(2): p. 111-119.
124. Turner, P.V., et al., *Administration of substances to laboratory animals: routes of administration and factors to consider*. J Am Assoc Lab Anim Sci, 2011. **50**(5): p. 600-13.
125. Costanzo, V., *Brca2, Rad51 and Mre11: performing balancing acts on replication forks*. DNA Repair (Amst), 2011. **10**(10): p. 1060-5.
126. Yahyapour, R., et al., *Radiation-induced Non-targeted Effect and Carcinogenesis; Implications in Clinical Radiotherapy*. J Biomed Phys Eng, 2018. **8**(4): p. 435-446.
127. Kominami, R. and O. Niwa, *Radiation carcinogenesis in mouse thymic lymphomas*. Cancer Sci, 2006. **97**(7): p. 575-81.
128. Li, N., H. Chen, and J. Wang, *DNA damage and repair in the hematopoietic system*. Acta Biochim Biophys Sin (Shanghai), 2022. **54**(6): p. 847-857.
129. Baum, C., et al., *Concise review: managing genotoxicity in the therapeutic modification of stem cells*. Stem Cells, 2011. **29**(10): p. 1479-84.
130. Mao, F., et al., *Plk1 Inhibition Enhances the Efficacy of BET Epigenetic Reader Blockade in Castration-Resistant Prostate Cancer*. Mol Cancer Ther, 2018. **17**(7): p. 1554-1565.
131. De Blasio, C., et al., *PLK1 targets NOTCH1 during DNA damage and mitotic progression*. J Biol Chem, 2019. **294**(47): p. 17941-17950.

132. Driscoll, D.L., et al., *Plk1 inhibition causes post-mitotic DNA damage and senescence in a range of human tumor cell lines*. PLoS One, 2014. **9**(11): p. e111060.
133. van Vugt, M.A., A. Bras, and R.H. Medema, *Polo-like kinase-1 controls recovery from a G2 DNA damage-induced arrest in mammalian cells*. Mol Cell, 2004. **15**(5): p. 799-811.
134. Mamely, I., et al., *Polo-like kinase-1 controls proteasome-dependent degradation of Claspin during checkpoint recovery*. Curr Biol, 2006. **16**(19): p. 1950-5.
135. van Vugt, M.A., et al., *A mitotic phosphorylation feedback network connects Cdk1, Plk1, 53BP1, and Chk2 to inactivate the G(2)/M DNA damage checkpoint*. PLoS Biol, 2010. **8**(1): p. e1000287.
136. Kemp, C.J., T. Wheldon, and A. Balmain, *p53-deficient mice are extremely susceptible to radiation-induced tumorigenesis*. Nat Genet, 1994. **8**(1): p. 66-9.
137. Utsuyama, M. and K. Hirokawa, *Radiation-induced-thymic lymphoma occurs in young, but not in old mice*. Exp Mol Pathol, 2003. **74**(3): p. 319-25.
138. Boulton, E., H. Cleary, and M. Plumb, *Myeloid, B and T lymphoid and mixed lineage thymic lymphomas in the irradiated mouse*. Carcinogenesis, 2002. **23**(6): p. 1079-85.

139. Ishihara, H., et al., *Induction of the expression of the interleukin-1 beta gene in mouse spleen by ionizing radiation*. Radiat Res, 1993. **133**(3): p. 321-6.
140. Finnberg, N., et al., *DR5 knockout mice are compromised in radiation-induced apoptosis*. Mol Cell Biol, 2005. **25**(5): p. 2000-13.
141. Rivina, L., M.J. Davoren, and R.H. Schiestl, *Mouse models for radiation-induced cancers*. Mutagenesis, 2016. **31**(5): p. 491-509.
142. Suttie, A.W., *Histopathology of the spleen*. Toxicol Pathol, 2006. **34**(5): p. 466-503.
143. Baratta, J.L., et al., *Cellular organization of normal mouse liver: a histological, quantitative immunocytochemical, and fine structural analysis*. Histochem Cell Biol, 2009. **131**(6): p. 713-26.
144. Menon, S.S., et al., *Ki-67 protein as a tumour proliferation marker*. Clin Chim Acta, 2019. **491**: p. 39-45.
145. Yang, Q., J. Jeremiah Bell, and A. Bhandoola, *T-cell lineage determination*. Immunol Rev, 2010. **238**(1): p. 12-22.
146. Mariotti, L.G., et al., *Use of the gamma-H2AX assay to investigate DNA repair dynamics following multiple radiation exposures*. PLoS One, 2013. **8**(11): p. e79541.
147. Ryu, S.H., et al., *Establishment of a mouse model of 70% lethal dose by total-body irradiation*. Lab Anim Res, 2016. **32**(2): p. 116-21.
148. Solaini, G., et al., *Evaluating mitochondrial membrane potential in cells*. Biosci Rep, 2007. **27**(1-3): p. 11-21.

149. Matsuzaki, S. and K.M. Humphries, *Selective inhibition of deactivated mitochondrial complex I by biguanides*. *Biochemistry*, 2015. **54**(11): p. 2011-21.
150. Giorgio, V., et al., *Dimers of mitochondrial ATP synthase form the permeability transition pore*. *Proc Natl Acad Sci U S A*, 2013. **110**(15): p. 5887-92.
151. Higgins, C.F., *ABC transporters: from microorganisms to man*. *Annu Rev Cell Biol*, 1992. **8**: p. 67-113.
152. Longo-Sorbello, G.S. and J.R. Bertino, *Current understanding of methotrexate pharmacology and efficacy in acute leukemias. Use of newer antifolates in clinical trials*. *Haematologica*, 2001. **86**(2): p. 121-7.
153. Baguley, B.C., *Classical and Targeted Anticancer Drugs: An Appraisal of Mechanisms of Multidrug Resistance*. *Methods Mol Biol*, 2016. **1395**: p. 19-37.
154. Pentikainen, P.J., P.J. Neuvonen, and A. Penttila, *Pharmacokinetics of metformin after intravenous and oral administration to man*. *Eur J Clin Pharmacol*, 1979. **16**(3): p. 195-202.
155. Foretz, M., et al., *Metformin: from mechanisms of action to therapies*. *Cell Metab*, 2014. **20**(6): p. 953-66.
156. Zhou, G., et al., *Role of AMP-activated protein kinase in mechanism of metformin action*. *J Clin Invest*, 2001. **108**(8): p. 1167-74.
157. Lin, H.Z., et al., *Metformin reverses fatty liver disease in obese, leptin-deficient mice*. *Nat Med*, 2000. **6**(9): p. 998-1003.

158. Marchesini, G., et al., *Metformin in non-alcoholic steatohepatitis*. Lancet, 2001. **358**(9285): p. 893-4.
159. Feng, X., et al., *Loss of Setd4 delays radiation-induced thymic lymphoma in mice*. DNA Repair (Amst), 2020. **86**: p. 102754.
160. Li, Z., et al., *Polo-like kinase 1 (Plk1) overexpression enhances ionizing radiation-induced cancer formation in mice*. J Biol Chem, 2017. **292**(42): p. 17461-17472.
161. Feng, X., et al., *Deletion of Mouse Setd4 Promotes the Recovery of Hematopoietic Failure*. Int J Radiat Oncol Biol Phys, 2020. **107**(4): p. 779-792.
162. TeSlaa, T. and M.A. Teitell, *Techniques to monitor glycolysis*. Methods Enzymol, 2014. **542**: p. 91-114.
163. Graham, G.G., et al., *Clinical pharmacokinetics of metformin*. Clin Pharmacokinet, 2011. **50**(2): p. 81-98.
164. Liu, Z., Q. Sun, and X. Wang, *PLK1, A Potential Target for Cancer Therapy*. Transl Oncol, 2017. **10**(1): p. 22-32.
165. Wilkinson, B., M.A. Hill, and J.L. Parsons, *The Cellular Response to Complex DNA Damage Induced by Ionising Radiation*. Int J Mol Sci, 2023. **24**(5).



**Scholastic and Professional Honors**

2022-2023

**Vice President of the Department of  
Toxicology and Cancer Biology  
Student Forum**

Department of Toxicology and Cancer  
Biology, University of Kentucky, College  
of Medicine

2021-2022

**President of the Department of  
Toxicology and Cancer Biology  
Student Forum**

Department of Toxicology and Cancer  
Biology, University of Kentucky, College  
of Medicine

2020-2021

**Vice President of the Department of  
Toxicology and Cancer Biology  
Student forum**

Department of Toxicology and Cancer  
Biology, University of Kentucky, College  
of Medicine

2022-2024

**Board Member**

Markey Cancer Center Trainee  
Advisory Council, University of  
Kentucky, College of Medicine

2022-2024

**Diversity Ambassador**

Department of Toxicology and Cancer  
Biology's Diversity, Equity, and  
Inclusion Committee, University of  
Kentucky, College of Medicine

**Publications**

1. Calderon, L. E.; Keeling, J. K.; Rollins, J.; Black, C. A.; **Collins, K.**; Arnold, N.; Vance, D. E.; Ndinguri, M. W. Pt-Mal-LHRH, a Newly Synthesized Compound Attenuating Breast Cancer Tumor Growth and Metastasis by Targeting Overexpression of the LHRH Receptor. *Bioconjugate Chem.* 2017. 28, 461–470. DOI: <https://doi.org/10.1021/acs.bioconjchem.6b00610>